Asymptotic Dynamical States in Networks of Kuramoto Oscillators with Inertia

MASTERARBEIT

zur Erlangung des akademischen Grades
Master of Science
(M. Sc.)
im Fach Physik

eingereicht an der
Mathematisch-Naturwissenschaftliche Fakultät
Institut für Physik
Humboldt-Universität zu Berlin

von
Herr B.Sc. Anton Plietzsch

Betreuung:

1. *Prof. Dr. Dr. h.c. mult. Jürgen Kurths*
2. *Dr. Frank Hellmann*

eingereicht am: *01. Dezember 2017*

Abstract

The Kuramoto model with inertia is a popular and straightforward model of the frequency dynamics in power grids. It has been widely used to study the stability and dynamics close to the global synchronous state. However, with an increasing share of renewable energies and the resulting decline of total system inertia the power system becomes more vulnerable to the emergence of undesirable dynamical states and large frequency deviations. The goal of this thesis is to approach this model from a viewpoint of nonlinear dynamics and analyze the different possible asymptotic dynamical states beside the synchronous fixed point. Analytical and numerical conditions for the existence of solitary states of single nodes as well as for coexisting synchronous clusters are derived.

Contents

List of Figures

It is by logic that we prove,
but by intuition that we discover.

– HENRI POINCARÉ [26]

Chapter 1

Motivation

The transition of the power system towards higher shares of renewable energy gives rise to major challenges regarding the dynamical stability and control of power grids. In grids with large numbers of conventional power plants frequency dynamics is stabilized by the rotating masses of the turbines providing kinetic energy. However, the increasing use of power electronic interfaced power sources like wind and solar leads to a reduction of conventional synchronous machines in the grid. This decrease of total system inertia reduces the dynamical stability and results in larger frequency gradients. This is already significantly affecting islanded power grids, notably in Ireland and Northern Ireland as well as in Great Britain. For that reason, there has been an upper limit of 50 % for the operation of power electronic interfaced power sources in the grid of Ireland. [5, 6]

Other challenges for operating power grids with high share of renewables are the intermittency of wind and solar power as well as the uneven geographical distribution of energy production and consumption, resulting in large exports of power from one area to another. During periods of strong winds there are for instance large power flows from Denmark and North Germany to Southern Europe. Under such circumstances there is an increased risk of transmission line overloads and the emergence of blackouts in the power system. Transmission system operators therefore apply the so-called N-1 criterion which guarantees that in case of a intended shut down or failure of an element the remaining elements in the grid are capable of coping the new operational situation without violating operational security limits. For the necessary calculations grid operators usually use static power flow equations that do not take the dynamics of the system into account. However, the reduction in total systems inertia and large power imbalances among different areas of the transmission grid gives rise to undesirable dynamical phenomena.

In particular, those power imbalances can trigger so-called inter-area oscillations where the synchronous machines in one area are oscillating against the machines in another. These oscillations are characterized by relatively low frequencies and small damping and are therefore difficult to control [28]. In case of large disturbances a power system may get into certain dynamical regimes where it does not return to the synchronous operation state but rather approaches certain non-synchronous oscillating states. Large uncontrolled oscillations in the power system are a severe threat for the grid stability and may cause large scale blackouts.

An example of such an incident is in the major disturbance in Western North American grid on August 10th in 1996 leading to a widespread outage of generation affecting about 7.5 million customers. Prior to the collapse there were large exports from the Pacific Northwest into California and from Canada into the Pacific Northwest and several 500 kV lines in Oregon short-circuited on trees. As a result, 13 hydro generating units operated by the power administration were removed from the grid by system protection relays followed by the beginning of an 0.224 Hz oscillation on the transmission system. At a certain point this oscillation became negatively damped and the growing amplitude reached a level were major interconnection lines failed and the grid was split into four unconnected islands. [23]

It is evident that analyzing the stability of the synchronous operating state as well as of undesirable dynamical states is of great importance. From the viewpoint of nonlinear dynamics the power system is a highly multi-stable system with a variety of different asymptotic states. The goal of this thesis is to identify such states and determine the conditions under which those are stable. The thesis is structured as follows: In Chapter 2 the common approach for modeling power grids as networks of oscillators is introduced. Chapter 3 deals with the stability of the synchronous state corresponding to the normal state of operation in power grids. In Chapter 4 some fundamental insights of the theory of linear periodic systems that will be used in the remaining chapters are outlined. Chapter 5 deals with the stability of the limit cycle state in the infinite bus model. In Chapter 6 a linearization approach for determining the stability of coexisting synchronized clusters with distinct frequency is introduced. A new limit cycle state for a certain class of nodes in the oscillator network is presented in Chapter 7. Finally, in Chapter 8 the results are summed up and suggestions for further research are given.

Chapter 2

Modeling Power Grids as Networks of Oscillators

Power grids are highly complex systems with nonlinear dynamics, a high dimensionality as well as a complicated network connectivity. The development of an appropriate model for such a system is therefore a great challenge. In recent years, there has been an increasing interest in the dynamics of power grids from the perspective of complex networks science [8, 17, 19, 21, 24, 31]. In this framework, the power grid is modeled as a network of nonlinear oscillators. This holistic approach allows for the detailed modeling of the dynamics of the whole grid with all its single components and their mutual interactions instead of an analysis restricted to single components. A central focus of the network theoretic approach lies on the influence of the network structure on the dynamics.

2.1 The Graph Representation of the Grid

Complex networks can be represented by *graphs* $\mathcal{G} = (\mathcal{N}, \mathcal{M})$, where $\mathcal{N}$ is a set of *nodes* and $\mathcal{M}$ is a set of *links* connecting pairs of nodes. Links are defined by the couple of nodes i and j they are connecting. They are also said to be *incident* to these nodes. We define n to be the total number of nodes and m to be the total number of links in the network. The nodes which are connected to a node i by a link are called *adjacent nodes* of i. A *walk* from node i to node j is an alternating sequence of adjacent nodes (or a sequence of nodes and links) that begins with i and ends with j. A *cycle* is a closed walk, of at least three nodes, in which no link is repeated. A *path* is a walk in which no node is visited more than once. The path of minimal length between two nodes is known as the *shortest path* d_{ij}. A *subgraph* $\mathcal{G}' = (\mathcal{N}', \mathcal{M}')$ is a graph with $\mathcal{N}' \subseteq \mathcal{N}$ and $\mathcal{M}' \subseteq \mathcal{M}$. Subgraphs in which every pair of nodes is connected by a path will be denoted as *clusters* $\mathcal{C}$. A cluster is called *component* of the graph if it is maximal, i.e. there exists no path between a node $i \in \mathcal{C}$ and any node $j \notin \mathcal{C}$. If a graph consists of exactly one component, it is said to be *connected*. A graph is called a *tree* if it is connected and has no cycles. [3, 20]

2.1.1 Adjacency and Incidence Matrix

Graphs can be represented by matrices. The *adjacency matrix* is a $n \times n$-matrix containing the information which pairs of nodes are connected.

$$A_{ij} = \begin{cases} 1 & \text{if } i \text{ and } j \text{ are connected,} \\ 0 & \text{otherwise.} \end{cases} \tag{2.1}$$

It can be used to calculate various global and local measures of the network structure. The degree of a node for example, is defined as the number other nodes it is connected to and can be calculated by

$$k_i = \sum_{j=1}^{n} A_{ij}. \tag{2.2}$$

For many real world networks and in particular for power grids, the links in the network are not identical. Depending on the the situation it might therefore be useful to introduce link weights w_{ij}. In the following, we assume these weights to be nonnegative and symmetric

$$w_{ij} = w_{ji} \geq 0. \tag{2.3}$$

Then, we can define a weighted adjacency matrix

$$A_{ij} = \begin{cases} w_{ij} & \text{if } i \text{ and } j \text{ are connected,} \\ 0 & \text{otherwise.} \end{cases} \tag{2.4}$$

Another representation of a graph is given by the *incidence matrix*. This is a $m \times n$-matrix containing the information which links $e = (i, j)$ are incident to which nodes

$$B_{ev} = \begin{cases} +1 & \text{if } v = i, \\ -1 & \text{if } v = j, \\ 0 & \text{otherwise.} \end{cases} \tag{2.5}$$

2.1.2 The Graph Laplacian

The *Laplacian* of a graph is a $n \times n$-matrix which is defined by

$$L = D - A, \tag{2.6}$$

where $D = \text{diag}(k_1, .., k_n)$ is the diagonal matrix with the node degrees on the diagonal. The single elements of L are thus given by

$$L_{ij} = \delta_{ij} \sum_{l=1}^{n} A_{il} - A_{ij}, \tag{2.7}$$

where δ_{ij} is the Kronecker delta. An alternative way of calculating the Laplacian is the factorization into the incidence matrix and its transpose.

$$L = B^T B \tag{2.8}$$

That this statement is true, will be shown in the following. When $i = j$,

$$[B^T B]_{ij} = \sum_{e=1}^{m} B_{ei}^2 = k_i. \tag{2.9}$$

Hence the diagonal elements of B^TB are equal to the degrees of the nodes. When $i \neq j$ and i and j are not connected,

$$[B^TB]_{ij} = \sum_{e=1}^{m} B_{ei}B_{ej} = 0, \tag{2.10}$$

since every link is non-incident to at least one of the nodes. On the other hand, when $i \neq j$ and there exists a link between those to nodes,

$$[B^TB]_{ij} = \sum_{e=1}^{m} B_{ei}Bej = -1. \tag{2.11}$$

It can easily be seen, that the equations (2.9)-(2.11) are equivalent to the definition of the Laplacian 2.6 and thus the factorization in (2.8) holds.

By definition the Laplacian is symmetric and therefore all its eigenvalues are real. Further, it can be shown that it is positive semidefinite and therefore all eigenvalues are nonnegative. These statements are also true for a weighted Laplacian if we assume the weights to be nonnegative and symmetric (2.3).

A real matrix is said to be positive semidefinite, if $x^TMx \geq 0$ for all real and nonzero vectors x. This can easily be proved for the Laplacian by making use of the factorization (2.8)

$$\boldsymbol{x}^TL\boldsymbol{x} = \boldsymbol{x}^TB^TB\boldsymbol{x} = (B\boldsymbol{x})^T(B\boldsymbol{x}) \geq 0. \tag{2.12}$$

We define the vector $\boldsymbol{v}^{(1)} = (1, ..., 1)^T$. From definition (2.7) follows directly that

$$[L\boldsymbol{v}^{(1)}]_i = \sum_{j=1}^{n} L_{ij} = 0. \tag{2.13}$$

Therefore, $\boldsymbol{v}^{(1)}$ is always an eigenvector of L with the corresponding eigenvalue $\lambda_1 = 0$.

Assume $\mathcal{G}$ and $\mathcal{H}$ are two graphs on the same node set with disjoint edge sets. Then, the adjacency matrix of the union of both graphs obviously fulfills $A_{\mathcal{G}\cup\mathcal{H}} = A_{\mathcal{G}} + A_{\mathcal{H}}$ and therefore by (2.7) additivity also holds for the Laplacian

$$L_{\mathcal{G}\cup\mathcal{H}} = L_{\mathcal{G}} + L_{\mathcal{H}}. \tag{2.14}$$

If we assume, that the node sets of $\mathcal{G}$ and $\mathcal{H}$ are also disjoint, then the union graph is unconnected and it can easily be seen that

$$L_{\mathcal{G}\cup\mathcal{H}} = \begin{pmatrix} L_{\mathcal{G}} & 0 \\ 0 & L_{\mathcal{H}} \end{pmatrix}. \tag{2.15}$$

If $L_{\mathcal{G}}$ has the eigenvectors $\boldsymbol{v}^{(i)}$ with eigenvalues λ_i and $L_{\mathcal{H}}$ has the eigenvectors $\boldsymbol{w}^{(i)}$ with eigenvalues μ_i then

$$\begin{pmatrix} L_{\mathcal{G}} & 0 \\ 0 & L_{\mathcal{H}} \end{pmatrix} \begin{pmatrix} \boldsymbol{v}^{(i)} \\ 0 \end{pmatrix} = \begin{pmatrix} \lambda_i\boldsymbol{v}^{(i)} \\ 0 \end{pmatrix} \tag{2.16}$$

and similarly

$$\begin{pmatrix} L_{\mathcal{G}} & 0 \\ 0 & L_{\mathcal{H}} \end{pmatrix} \begin{pmatrix} 0 \\ \boldsymbol{w}^{(i)} \end{pmatrix} = \begin{pmatrix} 0 \\ \mu_i \boldsymbol{w}^{(i)} \end{pmatrix}. \tag{2.17}$$

Hence, the eigenvectors of the union graph are given by $(\boldsymbol{v}^{(i)}, 0, ..., 0)^T$ and $(0, ..., 0, \boldsymbol{w}^{(i)})^T$ with the corresponding eigenvalues λ_i and μ_i. From this follows, that the number of zero eigenvalues of the Laplacian is at least the number of disjoint subgraphs. In fact, the dimension of the null space of L is exactly the number of connected components which will be shown in the following. For this purpose, we introduce the Laplacian of a single link

$$[L_e]_{ij} = \begin{cases} 1 & \text{if } i = j \\ -1 & \text{if } e \text{ is the link connecting } i \text{ and } j \\ 0 & \text{otherwise.} \end{cases} \tag{2.18}$$

Equation (2.14) implies that $L = \sum_{e=1}^{m} L_e$. If the graph is connected and $\boldsymbol{x}$ is a vector in the null space of L, i.e. $Lx = 0$ we get

$$0 = \boldsymbol{x}^T L \boldsymbol{x} = \sum_{e=1}^{m} \boldsymbol{x}^T L_e \boldsymbol{x} = \sum_{i,j=1}^{n} A_{ij}(x_i - x_j)^2. \tag{2.19}$$

Thus, $x_i = x_j$ for all connected nodes i and j. This means that all x_j are equal and every vector in the null space is a multiple of $\boldsymbol{v}^{(1)} = (1, ..., 1)^T$. For a connected graph the null space is therefore of dimension one and thus

$$\lambda_2 > 0. \tag{2.20}$$

In fact, λ_2 is an important measure for the network structure known as the algebraic connectivity.

2.1.3 Complex Network Measures

The structural properties of a complex network can be characterized by certain local and global network measures [3, 20]. One important example of a local measure is the degree of a node which was already introduced in (2.2). A corresponding global measure is the mean degree

$$\langle k \rangle = \frac{1}{n} \sum_{i=1}^{n} k_i = 2\frac{m}{n}, \tag{2.21}$$

which is proportional to the number of links m since the addition of a link increments the degree of two different nodes by one. The mean degree is therefore a measure for the link density of a network. However, this measure does not contain any information about the variance of degrees in a network. We define the degree distribution $P(k)$ as the probability distribution of degrees, i.e. the probability that a randomly chosen node has degree k is given by $P(k)$. This distribution is often very suitable for characterizing the structural properties of a graph. For random graphs where every pair of nodes is connected by a link with probability p the degree distribution is given by a binomial distribution [7]. On the other hand, the distribution of so-called scale-free networks follow a power law. Such networks are characterized by having a few nodes with very high degree (so-called hubs) [1].

Another important local measure is the clustering coefficient c_i that can be defined as the probability that two neighbors of a node are connected by a link

$$c_i = \frac{\sum_{j,k=1}^{n} A_{ij} A_{jk} A_{ki}}{k_i(k_i - 1)}. \tag{2.22}$$

The global clustering coefficient can be defined as the average of the local clustering coefficients and is related to the number of triangles in the network. Although clustering coefficients are mostly considered in the context of social networks they can also be of particular importance for the resilience of supply networks, since two nodes that are part of a triangle are still connected by a path of length $d_{ij} = 2$ in case of a failure of the link connecting those two nodes [25]. Shortest paths between pairs of nodes play an important role for the characterization of a network. The characteristic path length of a network is defined as the average shortest path length considering all pairs of nodes

$$L = \frac{\sum_{i,j=1}^{n} d_{ij}}{n(n-1)}. \tag{2.23}$$

Networks having both a large clustering coefficient and a short characteristic path length are known as 'small-world' networks [32].

2.1.4 Structural Properties of Power Grid Networks

Power grids typically have a very hierarchical structure. They are divided into several voltage levels that are characterized by different structural properties. While distribution grids (mid and low voltage level) are mostly characterized by tree-like structures, transmission grids (high voltage level) tend to have a more meshed network structure. The detailed structural properties of transmission grids of various sizes have been investigated using complex network analysis and statistical graph theory. This analysis was done with both real world topologies and synthetic grids (mostly IEEE bus systems) [24].

It turns out that transmission grids have a relatively sparse network structure with an average degree between $2 \leq \langle k \rangle \leq 4$. The degree distributions mostly follow an exponential distribution with specific parameters depending on the particular grid. The average path lengths are similar to those of random graphs of similar size while the clustering coefficients are typically higher but only for a few samples much higher than those of random graphs. Transmission grids are therefore not in general fulfilling the small-world property.

When studying the dynamics of power grids it is essential to use realistic network models having the same structural properties as real power grid topologies. For this purpose, we can for instance use simplified network models of real world power grids as well as synthetic benchmark grids like the IEEE test cases. However, in order to get a comprehensive understanding of the broad range of possible dynamical phenomena independent of a specific grid structure it is often useful to perform statistical analyses of large ensembles of network models with similar structural properties. For this purpose, a network growth model generating spatially embedded graphs with realistic topologies has been developed [30] recently. The model contains an initialization phase establishing a minimum spanning tree between a given set

of nodes and a growth phase extending the network by placing nodes at random and connecting them to the existing grid according to a heuristic cost/redundancy optimization. The parameters determining the growth phase can be chosen such that the mean degree and the degree distribution of the resulting network exactly fits those of realistic power grid topologies.

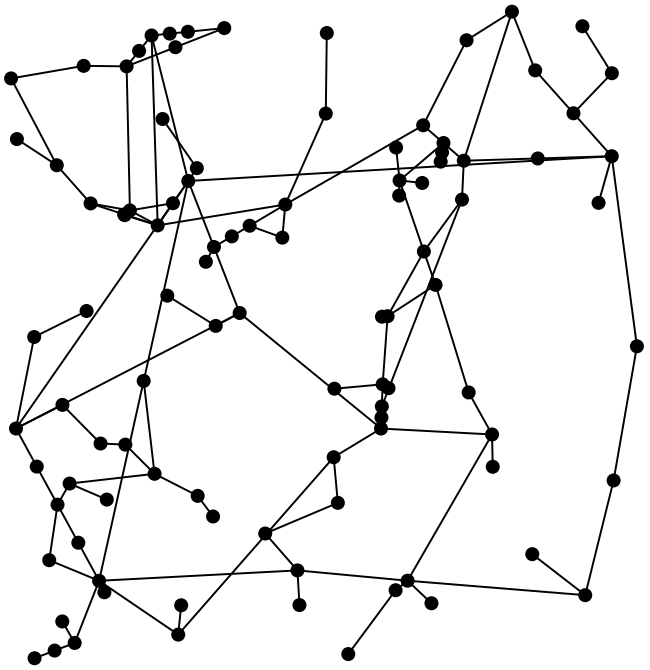

Figure 2.1: A spatially embedded network with $n = 100$ nodes and a topological structure similar to real world transmission grids. The graph was generated with the random growth model proposed in [30].

2.2 The Swing Equation

The synchronization of coupled nonlinear oscillators is a phenomenon that appears in many physical, biological and chemical systems. The most famous model for studying such systems is the celebrated Kuramoto model that assumes an infinite number of oscillators having their own frequencies being coupled by a sinusoidal function and a coupling constant [14, 27]. It turns out that frequency dynamics of power grids can be modeled by a second order model with a Kuramoto-like structure known as the Kuramoto model with inertia [8]. In the engineering literature this is known as the classical model or the swing equation [15]. It is used for analyzing the transient short time behavior of generators in a power grid, the so-called first swing.

2.2.1 Nonlinear Power Flow Equations

In this section we are going to derive the AC power flow equations in a transmission grid. Every line in the grid is characterized by its impedance $z_{ij} = r_{ij} + ix_{ij}$, where r_{ij} is the resistance and x_{ij} the reactance. The inverse of the impedance is called admittance $y_{ij} = z_{ij}^{-1}$, that can be written as $y_{ij} = g_{ij} + ib_{ij}$ with the conductance

g_{ij} and the susceptance b_{ij} that are given by

$$g_{ij} = \frac{r_{ij}}{|z_{ij}|^2} \tag{2.24}$$

$$b_{ij} = -\frac{x_{ij}}{|z_{ij}|^2}. \tag{2.25}$$

When we define the admittance between two unconnected nodes as $y_{ij} = 0$, we can interpret y_{ij} as elements of a weighted adjacency matrix of the power network as defined in Section 2.1.1. The current flowing on a line is given by Ohm's law

$$I_{ij} = y_{ij}(V_i - V_j). \tag{2.26}$$

The net current injection at a node can then be calculated by using Kirchhoff's first law

$$I_i = \sum_{j=1}^{n} I_{ij} = \sum_{j=1}^{n} y_{ij}(V_i - V_j) = V_i \sum_{l=1}^{n} y_{il} - \sum_{j=1}^{n} y_{ij} V_j \tag{2.27}$$

$$= \sum_{j=1}^{n} \delta_{ij} V_j \sum_{l=1}^{n} y_{il} - \sum_{j=1}^{n} y_{ij} V_j = \sum_{j=1}^{n} (\delta_{ij} \sum_{l=1}^{n} y_{il} - y_{ij}) V_j. \tag{2.28}$$

We can then define a nodal admittance matrix by

$$Y_{ij} = G_{ij} + iB_{ij} = \delta_{ij} \sum_{l=1}^{n} y_{il} - y_{ij}. \tag{2.29}$$

This matrix is basically a weighted Laplacian. With this, equation (2.28) can be written as

$$I = YV. \tag{2.30}$$

The complex voltage at node i is given by

$$V_i = |V_i| e^{i\phi_i}. \tag{2.31}$$

The complex power [9] can thus be calculated by

$$P_i + iQ_i = V_i \cdot I_i^* = V_i \sum_j Y_{ij}^* V_j^* = \sum_j |V_i||V_j|(G_{ij} - iB_{ij}) e^{i(\phi_i - \phi_j)}, \tag{2.32}$$

with the real and reactive powers

$$P_i = \sum_{j=1}^{n} |V_i||V_j| \left(G_{ij} \cos(\phi_i - \phi_j) + B_{ij} \sin(\phi_i - \phi_j) \right) \tag{2.33}$$

$$Q_i = \sum_{j=1}^{n} |V_i||V_j| \left(G_{ij} \sin(\phi_i - \phi_j) - B_{ij} \cos(\phi_i - \phi_j) \right). \tag{2.34}$$

In high voltage transmission grids, the line resistance can be neglected $r_{ij} \approx 0$ and thus, the conductance is $g_{ij} \approx 0$ and the susceptance becomes $b_{ij} \approx -x_{ij}^{-1}$. The nodal suceptance matrix is then given by

$$B_{ij} = -\delta_{ij} \sum_{l=1}^{n} x_{il}^{-1} + x_{ij}^{-1}, \tag{2.35}$$

and equation (2.33) reduces to

$$P_i = \sum_{j=1}^{n} \frac{|V_i||V_j|}{x_{ij}} \sin(\phi_i - \phi_j). \tag{2.36}$$

The power flow on a single line is therefore determined by the line reactance, voltage magnitude of the two nodes as well as the phase difference of the voltage angles

$$F_{ij} = \frac{|V_i||V_j|}{x_{ij}} \sin(\phi_i - \phi_j). \tag{2.37}$$

2.2.2 Dynamics of Synchronous Machines

Each generator i coupled to a grid is described by a power balance equation of the form

$$P_i^{source} = P_i^{acc} + P_i^{diss} + P_i^{trans}, \tag{2.38}$$

where P_i^{source} is the rate at which energy is fed into the generator. This energy is either accumulated as kinetic energy in the turbine P_i^{acc}, dissipated P_i^{diss} or transmitted into the grid P_i^{trans}. The change rate of kinetic energy is given by

$$P_i^{acc} = \frac{d}{dt}\left(\frac{1}{2} J_i (\omega_i^{gen})^2\right) = J_i \omega_i^{gen} \dot{\omega}_i^{gen}, \tag{2.39}$$

where J_i is the turbines total moment of inertia. The frequency of the generators turbine is close to the standard frequency Ω of the power system (either 50 or 60 Hz)

$$\omega_i^{gen}(t) = \Omega + \omega_i(t) \tag{2.40}$$

We therefore assume $\omega(t) \ll \Omega$ whereby (2.39) can be approximated as

$$P_i^{acc} \approx J_i \Omega \dot{\omega}_i. \tag{2.41}$$

The dissipation is proportional to the frequency deviation

$$P_i^{diss} = D_i \omega_i, \tag{2.42}$$

and the transmission is given by the nonlinear power flow as derived in the previous chapter

$$P_i^{trans} = \sum_{j=1}^{n} \frac{|V_i||V_j|}{x_{ij}} \sin(\phi_i - \phi_j). \tag{2.43}$$

Inserting (2.41), (2.42) and (2.43) into (2.38) yields

$$J_i \Omega \dot{\omega}_i = P_i^{source} - D_i \omega_i - \sum_{j=1}^{n} \frac{|V_i||V_j|}{x_{ij}} \sin(\phi_i - \phi_j). \tag{2.44}$$

The change rate of the phase angle ϕ_i is given by the rotation frequency ω and thus, in normalized units we finally get

$$\dot{\phi}_i = \omega_i \tag{2.45}$$

$$\dot{\omega}_i = P_i - \alpha_i \omega_i - \sum_{j=1}^{n} K_{ij} \sin(\phi_i - \phi_j), \tag{2.46}$$

with $P_i = P_i^{source}/(J_i\Omega)$, $\alpha_i = D_i/(J_i\Omega)$ and $K_{ij} = |V_i||V_j|/(x_{ij}J_i\Omega)$. Equations (3.1) and (3.2) are known as the swing equation or the Kuramoto model with inertia.

As mentioned in the beginning of the chapter, the swing equation is a second order model for the dynamics of the generator phase angles and frequencies omitting the dynamics of other variables such as voltages. Since the voltage dynamics in power grids is generally much slower than the frequency dynamics, the swing equation is an appropriate model for short timescales. However, it is far from clear that it shows the same asymptotic behavior compared to more realistic higher order models of synchronous machines. In a comparison between the swing equation and a fourth order model including voltage dynamics it has been shown that both models typically follow a similar trajectory [2]. Nevertheless, it turned out that there might exist a number of fixed points that are stable in second order but unstable in the fourth order model. Together with the slow voltage dynamics this has the effect that the trajectories of the fourth order model sometimes show a pseudo convergent behavior towards such fixed points until the voltage dynamics drives the system away into a different transient regime.

Chapter 3

Stability of the Synchronous State

In this chapter we want to analyze the global synchronous state of the swing equation where all oscillators in the network are rotating with the same frequency Ω. This state corresponds to the operating state of a power grid were all generators are synchronized with a frequency of typically either 50 or 60 Hz. Therefore, this state and its linear stability and dynamics has been well studied in the engineering literature. Recently, probabilistic measures have been proposed to assess the asymptotic and transient stability of the synchronous state against large perturbations.

3.1 Global Frequency Synchronization

The global synchronization of the swing equation

$$\dot{\phi}_i = \omega_i \tag{3.1}$$

$$\dot{\omega}_i = P_i - \alpha\omega_i - \sum_{j=1}^{n} K_{ij} \sin(\phi_i - \phi_j), \tag{3.2}$$

corresponds to the stationary state where all oscillators are rotating with the same constant frequency $\omega_i = \Omega$. By integration of (3.1) we get the phases

$$\phi_i = \Omega t + \phi_i^*, \tag{3.3}$$

where ϕ_i^* are constant phase shifts. From (3.2) follows that these phase shifts are constrained by the nonlinear equation system

$$0 = P_i - \alpha\Omega - \sum_{j=1}^{n} K_{ij} \sin(\phi_i^* - \phi_j^*). \tag{3.4}$$

When summing (3.4) over all i, the sum over the sines of the phase differences vanishes since the sine is an odd function and we get

$$0 = \sum_{i=1}^{n} P_i - \sum_{j=1}^{n} \alpha\Omega \tag{3.5}$$

and thus the global frequency is given by

$$\Omega = \frac{\sum_{j=1}^{n} P_i}{n\alpha}. \tag{3.6}$$

3.2 Reference Frames and Symmetries

When the phase angles ϕ_i of the oscillators are measured relative to a certain reference angle ϕ_r

$$\phi_i' = \phi_i - \phi_r, \tag{3.7}$$

the swing equation (3.1) and (3.2) remains unchanged. This implies, that there is a rotational symmetry of the system that reduces the dimension of the dynamical system by one. Here we assumed, that the network is connected, i.e. there exists only one component. In general, the number of rotational symmetries is equal to the number of components of the network since for every component we can choose an arbitrary reference angle without changing the dynamics of the system.

Similarly, we can measure the frequencies ω_i relative to a reference frequency ω_r

$$\omega_i' = \omega_i - \omega_r \tag{3.8}$$
$$\phi_i' = \phi_i - \omega_r t. \tag{3.9}$$

Inserting this into (3.2) yields

$$\dot{\omega}_i' = P_i - \omega_r - \alpha\omega_i' - \sum_{j=1}^{n} K_{ij} \sin(\phi_i' - \phi_j'). \tag{3.10}$$

Thus, by scaling the power feed-in as

$$P_i' = P_i - \alpha\omega_r, \tag{3.11}$$

the structure of the swing equation remains unchanged.

A special case is the so called co-rotation frame, were the frequency of the global synchronous state is chosen as the reference frequency $\omega_r = \Omega$. Using (3.6), the power feed-ins are then given by

$$P_i' = P_i - \frac{1}{n}\sum_{j=1}^{n} P_j. \tag{3.12}$$

Consequently, in the co-rotating frame the network is always power-balanced, i.e. $\sum_{j=1}^{n} P_i' = 0$.

Finally, we want to analyze the dynamics of the mean frequency

$$\langle\omega\rangle = \frac{1}{n}\sum_{i}^{n} \omega_i. \tag{3.13}$$

Averaging the swing equation (3.2) over all oscillators yields

$$\langle\dot{\omega}\rangle = -\alpha\langle\omega\rangle \tag{3.14}$$

and thus, after any perturbation the mean frequency decays exponentially

$$\langle\omega(t)\rangle = \langle\omega(0)\rangle e^{-\alpha t}. \tag{3.15}$$

3.3 Linear Stability

In this section we want to analyze the dynamics of the swing equation close to the global synchronous state of the system. Therefore, we write the phase as

$$\phi_i(t) = \phi_i^* + \delta\phi_i, \tag{3.16}$$

where ϕ_i^* are the solutions of the power flow equations

$$P_i = \sum_{j=1}^{N} K_{ij} \sin(\phi_i^* - \phi_j^*) \tag{3.17}$$

for the synchronous state and $\delta\phi_i \ll 1$ are small deviations. Here, we assume that we are in the co-rotating frame such that the global frequency $\omega_{global} = 0$ and thus $\delta\dot{\phi}_i = \omega_i$. With this ansatz, we can linearize the sine function in (3.2) and get

$$\dot{\omega}_i = -\alpha\omega_i - \sum_{j=1}^{N} K_{ij} \cos(\phi_i^* - \phi_j^*)(\delta\phi_i - \delta\phi_j) \tag{3.18}$$

We can define a dynamical Laplacian

$$L_{ij} = -\delta_{ij} \sum_{l=1}^{N} K_{il} \cos(\phi_i^* - \phi_l^*) + K_{ij} \cos(\phi_i^* - \phi_j^*), \tag{3.19}$$

that is basically a negative Laplacian of the network structure, with coupling strengths weighted by the cosine of the phase angle differences in the synchronous state. With this matrix, equation (3.18) can be written as

$$\delta\dot{\omega}_i = -\alpha\omega_i + \sum_{j=1}^{N} L_{ij}\delta\phi_j. \tag{3.20}$$

If we define $\delta\boldsymbol{\phi} = (\delta\phi_1, ..., \delta\phi_N)^T$ and $\boldsymbol{\omega} = (\omega_1, ..., \omega_N)^T$, the whole linearized dynamical system can be written as

$$\begin{pmatrix} \delta\dot{\boldsymbol{\phi}} \\ \dot{\boldsymbol{\omega}} \end{pmatrix} = \begin{pmatrix} 0 & \mathbb{1} \\ L & -\alpha\mathbb{1} \end{pmatrix} \begin{pmatrix} \delta\boldsymbol{\phi} \\ \boldsymbol{\omega} \end{pmatrix}. \tag{3.21}$$

Thus, we have a $2N$-dimensional first order differential equation system of the form

$$\dot{x}(t) = Ax, \tag{3.22}$$

where

$$A = \begin{pmatrix} 0 & \mathbb{1} \\ L & -\alpha\mathbb{1} \end{pmatrix} \tag{3.23}$$

is the Jacobian matrix. The general solution of (3.22) is

$$x(t) = e^{At}x(0), \tag{3.24}$$

where e^{At} is a matrix exponential. The dynamics of the system is thus determined by the eigenvalues σ_i and eigenvectors $\boldsymbol{w}^{(i)}$ of the Jacobian. These are closely related

to the eigenvalues and eigenvectors of the Laplacian defined in (3.19) as is shown in the following.

$$A \cdot \boldsymbol{w} = \begin{pmatrix} 0 & \mathbb{1} \\ L & -\alpha\mathbb{1} \end{pmatrix} \begin{pmatrix} \boldsymbol{v} \\ \boldsymbol{u} \end{pmatrix} = \begin{pmatrix} \boldsymbol{u} \\ L \cdot \boldsymbol{v} - \alpha \boldsymbol{u} \end{pmatrix} = \sigma \begin{pmatrix} \boldsymbol{v} \\ \boldsymbol{u} \end{pmatrix} \tag{3.25}$$

From this we get

$$\boldsymbol{u} = \sigma \boldsymbol{v} \tag{3.26}$$

$$L \cdot \boldsymbol{v} = \sigma(\alpha + \sigma)\boldsymbol{v}, \tag{3.27}$$

and thus, $\boldsymbol{v}$ is an eigenvector of the Laplacian. If we denote the corresponding eigenvalue by λ, the eigenvalues of the Jacobian are solutions to the quadratic equation

$$\sigma^2 + \alpha\sigma - \lambda = 0. \tag{3.28}$$

and hence given by

$$\sigma_{\pm} = -\frac{\alpha}{2} \pm \sqrt{\frac{\alpha^2}{4} + \lambda}. \tag{3.29}$$

Since the Laplacian always has a zero eigenvalue, the Jacobian always has two real eigenvalues $\sigma 1 = 0$ and $\sigma_2 = -\alpha$ corresponding to the eigenvectors $\boldsymbol{w} = (1, ..., 0, ...)^T$ and $\boldsymbol{w} = (1, ..., -\alpha, ...)^T$. The eigenvalue λ_1 reflects the rotational symmetry of a homogeneous constant phase shift discussed in the previous section. The second eigenvalue corresponds to a a homogeneous shift in the frequencies that leaves the power flow unaffected and decays exponentially.

When all phase angle difference between adjacent nodes fulfill $|\phi_i^* - \phi_j^*| < \pi/2$, the Laplacian has only non-positive eigenvalues. In that case, the eigenvalues of the Jacobian all have negative real parts and the synchronous fixed point is linear stable. Laplacian eigenvalues with $|\lambda| > \alpha^2/4$ have an imaginary part and correspond to damped oscillating modes. On the other hand, eigenvalues with $|\lambda| < \alpha^2/4$ correspond to overdamped and therefore slowly declining modes.

3.4 Stability against Large Perturbations

In the previous section we analyzed the linear stability of the synchronous state corresponding to small perturbations of that state. The stability against large perturbations is usually assessed by using Lyapunov functions. However, for multi-stable systems having a large number of degrees of freedom and possibly complicated dynamics, such functions are usually hard to find. Therefore, an alternative approach for determining the stability against large perturbations by using probabilistic measures has been developed recently. Two examples of such measures are basin stability B measuring the fraction of initial states for which the trajectories approach a desirable asymptotic state [18] and survivability S measuring the fraction of initial states for which the trajectories stay inside a desirable region of the phase space [12]. Basin stability and survivability are rather complementary measures, the former focusing on the asymptotic and the latter on the transient behavior of the dynamics.

In case of a power grid the desirable attracting state would be the synchronous fixed point and the desirable region could for example be confined by certain frequency bounds. The two measures can then be interpreted as the probabilities that

the system returns to the stable fixed point respectively stays within the predefined frequency bounds after a random perturbation. The advantage of such a probabilistic definition of stability measures is that they can be easily computed using Monte Carlo sampling methods. This is done by numerical integrations of the system for an ensemble of randomly chosen initial conditions and an evaluation whether the resulting trajectories return to the stable fixed point respectively stay inside the predefined frequency boundaries. The estimation of basin stability and survivability can thus be computed by Bernoulli trials. For a sample size of N trials the standard error is given by

$$SEM = \sqrt{\frac{p(1-p)}{N}}, \tag{3.30}$$

were p is the estimate of either the basin stability B or the survivability S.

3.4.1 Basin Stability

The idea of the basin stability concept is to relate the stability of a desirable attractive state to the volume of the basin of attraction in the phase space X of the dynamical system. In a power grid the desired state corresponds to the stable fixed point $X^* \subset X$ of global synchronization ($\Omega = 0$ in the co-rotating frame)

$$X^* = \{(\phi_1^*, ..., \phi_N^*, 0, ..., 0)\}. \tag{3.31}$$

The basin of attraction $X^B \subseteq X$ of the state $X^* \subseteq X^B$ is given by all initial states from which the system asymptotically converges towards X^*

$$X^B = \{x(0) \in X \mid \lim_{t\to\infty} x(t) \in X^*\}. \tag{3.32}$$

Given the probability measure μ of initial conditions that can be interpreted as a probability distribution of possible perturbations, the basin stability is defined as

$$B_\mu = \mu(X^B). \tag{3.33}$$

Assuming a uniform distribution of initial conditions in a subset $X^0 \subset X$, the measure μ is proportional to the volume and the basin stability is then given by the ratio

$$B = \frac{\mathrm{Vol}(X^B \cap X^0)}{\mathrm{Vol}(X^0)}. \tag{3.34}$$

In case of networked systems like power grids, it is useful to define a single node basin stability B_i for studying localized perturbations of a single node in the network. This can be achieved by drawing the initial conditions from $X^0 \subset X_i$, where $X_i \subset X$ is the subset of the phase space spanned by the the variables corresponding to node i.

Using the single node basin stability estimate it was possible to relate the stability of the synchronous state against large local perturbations to certain local network structures [17, 29]. The nodes can basically be categorized into three different classes: nodes with poor stability ($S_i < 0.3$), with fair stability ($0.3 \leq S_i \leq 0.95$) and with high stability ($S_i > 0.95$). The majority of nodes has a fair value of basin stability. A perturbation of these nodes can induce only one sort of non-synchronous asymptotic state: the affected node becomes strongly desynchronized and oscillates about its natural frequency whereas all other nodes remain almost synchronous.

For nodes with high values of basin stability this desynchronized state is not asymptotically stable. On the other hand, for nodes with poor values of basin stability there exist more than one stable non-synchronous state. It turns out, that this particularly applies to nodes that are connected to nodes of degree one or tree-like appendices (dead ends and dead trees) [17]. Perturbations that hit such a node can induce multiple asymptotic states where one or several nodes in the tree structure become desynchronized. In contrast, so-called detour nodes (nodes of degree $k = 2$ that are part of a triangle) always have at least fair values of basin stability, i.e. a perturbation of such a node almost never induces a non-synchronous state where a node other than the perturbed one becomes desynchronized [29].

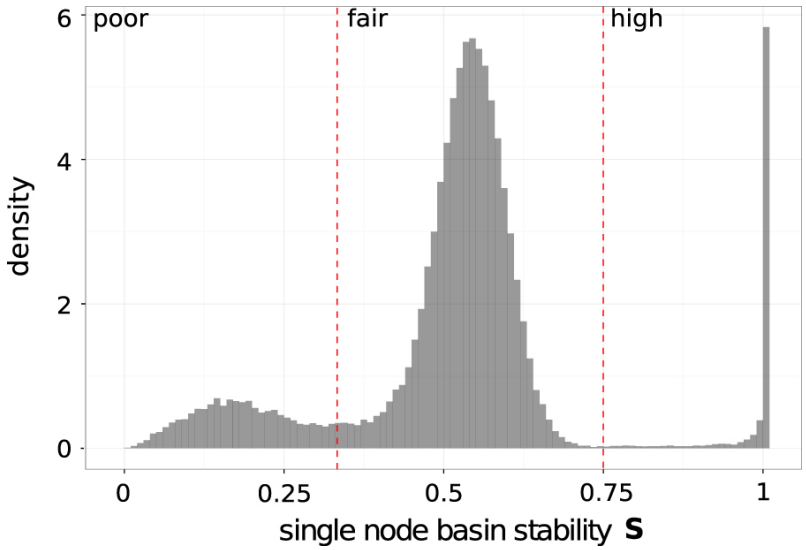

Figure 3.1: Distribution of single node basin stabilities for a network generated with the random growth model for power grids [30]. The dashed lines delimit the classes of poor (14%), fair (79%) and high (7%) basin stability. (Figure by Schultz et al. (2014) [29] / CC BY 3.0)

3.4.2 Survivability

The definition of the survivability strongly depends on the choice of the desirable region $X^+ \subseteq X$ in the phase space X. For the frequency dynamics of a power grid where the state of every synchronous machine is determined by a phase angle ϕ_i and a frequency ω_i the desirable region can be defined as the set of states where all deviations of the individual frequencies ω_i from the global frequency of the synchronous state ($\Omega = 0$ in the co-rotating frame) are smaller than a certain maximally tolerable deviation $\omega^+ > 0$

$$X^+ = \{(\phi_1, ..., \phi_N, \omega_1, ..., \omega_N) \mid |\omega_i| \leq \omega^+ \forall i\}. \tag{3.35}$$

The finite-time basin of survival $X_t^S \subseteq X^+$ is defined as the set of initial conditions $x(0) \in X$ for which the entire trajectory $x(t')$ over the time interval $[0, t]$ lies in X^+

$$X_t^S = \{x(0) \in X \mid x(t') \in X^+ \forall 0 \leq t' \leq t\}. \tag{3.36}$$

The infinite-time basin of survival is obtained by taking the limit $X^S = \lim_{t\to\infty} X_t^S$. Given the probability measure μ of initial conditions, the survivability is defined as

$$S_\mu = \mu(X^S). \tag{3.37}$$

Again, assuming a uniform distribution of initial conditions in a subset $X^0 \subset X$, the measure μ is proportional to the volume and the survivability is given by the ratio

$$S = \frac{\mathrm{Vol}(X^S \cap X^0)}{\mathrm{Vol}(X^0)}. \tag{3.38}$$

Similar to the single node basin stability we can define a single node survivability S_i by drawing the initial conditions from $X^0 \subset X_i$. Note that although the perturbation is local the violation of the frequency constraint by any arbitrary node is counted as not survived.

The single node survivability is strongly related to the degree of the perturbed node as well as to the degree of its neighbors. With a simple classification of the nodes based on these two measures the strong dependence of the transient behavior on the local network structure has been shown [22]. Generally, nodes with high degree have a significantly lower survivability. For nodes with degree one that are coupled to a high degree node even a new type of asymptotic has been observed. The properties of that novel state will be analyzed in Chapter 7.

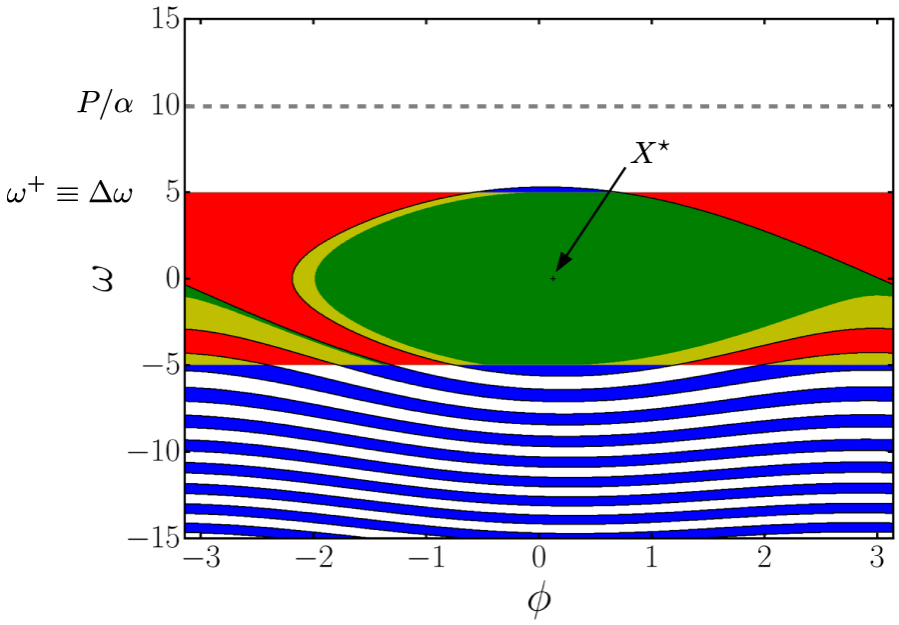

Figure 3.2: Phase space of the damped pendulum with torque. Areas in green, blue and yellow mark the basin of attraction of the fixed point. The desirable frequency band is colored in red, yellow and green. The infinite-time basin of survival is given by the green area. Trajectories starting in the yellow region converge towards the fixed point but their transients leaves the desirable region. (Figure by Nitzbon et al. (2017) [22] / CC BY 3.0)

Chapter 4

Theory of Linear Time-Varying Systems

The stability of fixed points in a nonlinear system can be determined by linearizing the equations around the fixed point. Since fixed point solutions by definition do not depend on time, this leads to a linear system with constant coefficients. The stability of such systems can be obtained by evaluating the eigenvalue spectrum. When analyzing the stability of limit cycles, a similar approach can be made by linearizing the system around the periodic solution. However, in this case we end up with a linear but periodically time dependent system. Determining the stability of such systems is much more difficult. In this chapter, we will introduce some essential theorems of the theory of linear periodic systems that will be helpful in the subsequent chapters.

4.1 Stability of Linear Systems

At first, we will analyze the stability of general linear time-varying systems of the form

$$\dot{x} = A(t)x. \tag{4.1}$$

This section is in a large part based on Chapter 3 of Hale's *Ordinary Differential Equations* [11].

An $n \times n$-matrix $X(t)$ is said to be a *matrix solution* of (4.1) if each column satisfies (4.1). $X(t)$ is called a *fundamental matrix solution* if its columns are linear independent, i.e. $\det(X(t)) \neq 0$. If $X(t)$ is any fundamental matrix solution of (4.1), then a general solution of (4.1) is $X(t)c$ where c is an arbitrary n-dimensional vector.

4.1.1 Homogeneous Linear Systems

Consider an ordinary differential equation $\dot{x} = f(x,t)$ having a fixed point $x = 0$, i.e. $f(0,t) = 0$ for $t \in [0,\infty)$.

1. The fixed point is called *Lyapunov stable* if for any $\epsilon > 0$ and any $t_0 \geq 0$ there is a $\delta = \delta(t_0, \epsilon)$, such that $|x(t_0)| < \delta$ implies $|x(t, t_0, x(t_0))| < \epsilon$ for $t \in [t_0, \infty)$.

2. The fixed point is called *uniformly stable* if it is Lyapunov stable and δ can be chosen independent of t_0.

3. The fixed point is called *asymptotically stable* if it is Lyapunov stable and there exists a $\delta = \delta(t_0)$ such that $x(t_0) < \delta$ implies $|x(t)| \to 0$ as $t \to \infty$.

4. The fixed point is called *uniformly asymptotically stable* if it is uniformly stable, δ in the definition of asymptotic stability can be chosen independent of t_0 and for every ϵ there is a $T(\epsilon) > 0$ such that $x(t_0) < \delta$ implies $|x(t, t_0, x(t_0))| < \epsilon$ if $t \geq t_0 + T(\epsilon)$.

5. The fixed point is called *unstable* if it is not Lyapunov stable.

For linear systems of the form (4.1) we can derive conditions for stability.

Theorem 4.1.1. *Let $X(t)$ be a fundamental matrix solution of (4.1) and let β be any number in $(-\infty, \infty)$. The system (4.1) is*

1. Lyapunov stable *for any t_0 in $(-\infty, \infty)$ if and only if there is a $K = K(t_0) > 0$ such that*

$$|X(t)| \leq K, \quad \text{for all } t_0 \leq t < \infty; \tag{4.2}$$

2. uniformly stable *for $t_0 \geq \beta$ if and only if there is a $K = K(\beta) > 0$ such that*

$$|X(t)X^{-1}(s)| \leq K, \quad \text{for all } t_0 \leq s \leq t < \infty; \tag{4.3}$$

3. asymptotically stable *for any t_0 in $(-\infty, \infty)$ if and only if*

$$|X(t)| \to 0 \text{ as } t \to \infty; \tag{4.4}$$

4. uniformly asymptotically stable *for $t_0 \geq \beta$ if and only if it is* exponentially stable*, i.e. there are $K = K(\beta) > 0$ and $\eta = \eta(\beta) > 0$ such that*

$$|X(t)X^{-1}(s)| \leq Ke^{-\eta(t-s)}, \quad \text{for all } t_0 \leq s \leq t < \infty. \tag{4.5}$$

Proof. See [11, p. 84–85]. □

A special case of (4.1) are linear systems with constant coefficients

$$\dot{x} = Ax. \tag{4.6}$$

For such systems the stability depends only on the eigenvalues of the matrix A.

Theorem 4.1.2. *A necessary and sufficient condition for the system (4.6) to be asymptotically stable is that all eigenvalues of A have negative real parts. If this is the case, there exist positive constants K, η such that*

$$|e^{At}| \leq Ke^{-\eta t}, \quad \text{for all } t \leq 0. \tag{4.7}$$

Proof. See [11, p. 100]. □

4.1.2 Perturbed Linear Systems

In this section we want to study non-homogeneous non-autonomous systems of the form

$$\dot{x} = A(t)x + f(x,t), \tag{4.8}$$

where $f(x,t)$ can be regarded as a perturbation of the homogeneous linear system (4.1).

Theorem 4.1.3. *If $X(t)$ is a fundamental matrix solution of (4.1) then every solution of (4.8) is given by*

$$x(t) = X(t)X^{-1}(t_0)x(t_0) + \int_{t_0}^{t} X(t)X^{-1}(s)f(x(s),s)ds, \tag{4.9}$$

for any real number $t_0 \in (-\infty, \infty)$.

Proof. See [11, p. 81] and [4, p. 156]. □

Equation (4.9) is known as the *variation of parameters formula*. Using this formula we can derive conditions for the stability of (4.8). We will consider two separate cases:

1. Perturbation of the form $f(x,t) = B(t)x$, where $B(t)$ is a $n \times n$ continuous matrix function.
2. Bounded perturbations $f(x,t) = f(t)$, i.e. with $|f(t)| < C$.

In the first case, equation (4.8) takes the form

$$\dot{x} = [A(t) + B(t)]x. \tag{4.10}$$

For the proof of the following theorem, we will need Grönwalls Inequality.

Lemma 4.1.1 (Grönwall's Inequality)**.** *If α is a real constant, $\beta(t) \geq 0$ and $\phi(t)$ are continuous real functions for $a \leq t \leq b$ satisfying*

$$\phi(t) \leq \alpha + \int_a^t \beta(s)\phi(s)ds \tag{4.11}$$

then

$$\phi(t) \leq e^{\int_a^t \beta(s)ds}. \tag{4.12}$$

Proof. See [11, p. 36] □

Theorem 4.1.4. *Suppose β is given in $(-\infty, \infty)$ and the homogeneous system (4.1) is uniformly asymptotically stable for $t_0 \geq \beta$. If the matrix function $B(t)$ satisfies*

$$\int_{t_0}^{t} |B(s)|ds \leq \gamma(t - t_0) + \tau, \quad \text{for all } t \geq t_0 \geq \beta \tag{4.13}$$

for some constants $\gamma = \gamma(\beta) > 0$, $\tau = \tau(\beta)$, then there is a threshold $r > 0$ such that the system (4.10) is uniformly asymptotically stable if $\gamma < r$.

Proof. If $X(t)$ is a fundamental matrix solution of the homogeneous system (4.1) and the homogeneous system is uniformly asymptotically stable for $t_0 \geq \beta$, then there are constants $K = K(\beta) > 0$, $\eta = \eta(\beta) > 0$ such that (4.5) is satisfied. Inserting this into the variation of parameters formula (4.9) we get

$$|x(t)| \leq Ke^{-\eta(t-t_o)}|x(t_0)| + K\int_{t_0}^{t} e^{-\eta(t-s)}|B(s)| \cdot |x(s)|ds. \tag{4.14}$$

If $z(t) = e^{\eta t}|x(t)|$, this implies

$$z(t) \leq Kz(t_0) + \int_{t_0}^{t} K|B(s)|z(s)ds. \tag{4.15}$$

Applying Grönwalds inequality yields

$$z(t) \leq Ke^{k\int_{t_0}^{t}|B(s)|ds}z(t_0). \tag{4.16}$$

Using the condition (4.13) we finally get

$$|x(t)| \leq Ke^{K\tau}|x(t_0)|e^{-(\eta-K\gamma)(t-t_0)}. \tag{4.17}$$

Thus, if $r = \eta/K$ and $\gamma < r$, the system (4.10) is uniformly asymptotically stable. □

For perturbations of the form $f(x,t) = f(t)$ equation (4.8) takes the form

$$\dot{x} = A(t)x + f(t). \tag{4.18}$$

Note, that $x = 0$ is not a fixed point of (4.18). Therefore, we can only make statements about the boundedness of the solutions.

Theorem 4.1.5. *Suppose β is given in $(-\infty, \infty)$ and the homogeneous system (4.1) is uniformly asymptotically stable for $t_0 \geq \beta$. If the continuous function $f(t)$ is bounded, then the non-homogeneous system (4.18) is bounded.*

Proof. If $X(t)$ is a fundamental matrix solution of (4.1), then the condition for uniform asymptotic stability (4.5) and the variation of constants formula (4.9) imply that for any solution of (4.18)

$$|x(t)| \leq Ke^{-\eta(t-t_0)}|x(t_0)| + K\int_{t_0}^{t} e^{-\eta(t-s)}|f(s)|ds. \tag{4.19}$$

When $f(t)$ is bounded, i.e. $|f(t)| \leq C$ then

$$|x(t)| \leq Ke^{-\eta(t-t_0)}|x(t_0)| + KC\int_{t_0}^{t} e^{-\eta(t-s)}ds. \tag{4.20}$$

and thus, any solution of (4.18) is bounded for any $t \geq t_0$ by

$$|x(t)| \leq K|x(t_0)| + \frac{KC}{\eta}. \tag{4.21}$$

□

4.2 Floquet Theory

In this section we will study periodic linear systems

$$\dot{x} = A(t)x, \quad A(t+T) = A(t). \tag{4.22}$$

The theoretical framework for such systems is the so called Floquet theory. This section is in a large part based on Chapter 2.4 of Chicone's *Ordinary differential equations with applications* [4].

Theorem 4.2.1 (Floquet's Theorem)**.** *If $X(t)$ is a fundamental matrix solution of (4.22), then there exist a periodic matrix function $P(t+T) = P(t)$ and a matrix B such that*

$$X(t) = P(t)e^{tB}. \tag{4.23}$$

The matrix B is given by

$$e^{TB} = X(0)^{-1}X(T). \tag{4.24}$$

Proof. See [4, p. 189] □

The decomposition of the fundamental matrix into a periodic and an exponential part $X(t) = P(t)e^{tB}$ is called *Floquet normal form.* The matrix $e^{TB} = X(0)^{-1}X(T)$ is called *mondronomy matrix.* The eigenvalues of the mondronomy matrix are called *characteristic multipliers* of the system. A complex number μ is called *characteristic exponent* or *Floquet exponent*, if ρ is a characteristic multiplier and $e^{\mu T} = \rho$. Note, that there are exactly n characteristic multipliers but infinitely many Floquet exponents, since $\mu + 2\pi ik/T$ is a Floquet exponent for every integer k if $e^{\mu T} = \rho$.

Theorem 4.2.2. *If μ is a Floquet exponent of (4.22) and $\rho = e^{\mu T}$ the corresponding characteristic multiplier, then there is a nontrivial solution of the form*

$$x(t) = e^{\mu t}p(t), \tag{4.25}$$

where $p(t+T) = p(t)$ is a periodic function and $x(t+T) = \rho x(t)$.

Proof. See [4, p. 198] □

The stability of the zero solution of (4.22) can be determined by the Floquet multipliers.

Theorem 4.2.3. *The solution $x(t) = 0$ of the system (4.22) is*

1. uniformly asymptotically stable*, if all characteristic multipliers have modulus less than one (or equivalently all Floquet exponents have negative real part).*
2. unstable*, if at least one characteristic multiplier has modulus greater than one (or equivalently at least one Floquet exponent has positive real part).*

Proof. See [11, p. 120] and [4, p. 194–195] □

Note, that the stability of the zero solution is not determined by the eigenvalues of $A(t)$. Particularly, if λ_i is an eigenvalue of $A(t)$, the condition $\Re(\lambda_i) < 0$ for all λ_i does not ensure the stability of the zero solution which can be seen from the following counter example

$$A(t) = \begin{pmatrix} -1 + \frac{3}{2}\cos^2(t) & 1 - \frac{3}{2}\sin(t)\cos(t) \\ -1 - \frac{3}{2}\sin(t)\cos(t) & -1 + \frac{3}{2}\sin^2(t) \end{pmatrix}. \tag{4.26}$$

The matrix has the time independent eigenvalues $1/4(-1 \pm \sqrt{7}i)$ but on the other hand

$$x(t) = e^{t/2} \begin{pmatrix} -\cos(t) \\ \sin(t) \end{pmatrix} \tag{4.27}$$

is a solution of system (4.22) with matrix (4.26) and thus the system is unstable.

Although the stability of the system is fully determined by the Floquet exponents, it is not at all clear how to find the eigenvalues of the mondronomy matrix without solving the entire system. Nevertheless, the theory provides a straightforward approach to determine the Floquet exponents numerically as follows:

1. Choose initial conditions for the fundamental matrix solution $\Phi(0)$.
2. Integrate the system (4.22) over one period T to get $X(T)$.
3. Compute the eigenvalues λ_i of the mondronomy matrix $e^{TB} = X(0)^{-1}X(T)$
4. Calculate the corresponding Floquet exponent

$$\mu_i = \frac{1}{T} \ln(\lambda_i). \tag{4.28}$$

For the special case of the so called Hill equation there exists an alternative approach for determining the stability of the system that will be discussed in the next section.

4.3 The Mathieu Equation

An important example of a linear periodic system is second order Hill equation

$$\ddot{x} + J(t)x = 0, \tag{4.29}$$

where $J(t) = \sum_{l=-\infty}^{\infty} \theta_l e^{2ilt}$ is an even function with period $T = \pi$. Depending on the specific shape of $J(t)$, solutions are either bounded for all time, or the amplitude of the oscillations in solutions grows exponentially. The stability of the solutions is determined by the Floquet exponents. Hill showed that the solutions can be expressed in terms of determinants of infinite matrices [13]. In the following we will outline this method for a special case of (4.29) with only one harmonic mode, known as the Mathieu equation

$$\ddot{x} + [\theta_0 + 2\theta_1 \cos(2t)]x = 0. \tag{4.30}$$

4.3.1 Inifinite Determinants

From Floquet theory we know that solutions of (4.30) can be separated into an exponential and a periodic part

$$x(t) = e^{\mu t} \sum_{l=-\infty}^{\infty} b_l e^{2ilt}. \tag{4.31}$$

When the Floquet exponent μ has negative real part, then the solution is asymptotically stable. Substituting (4.31) into the differential equation (4.30) we obtain an infinite set of equations

$$[(\mu + 2il)^2 + \theta_0]b_l + \theta_1 b_{l+1} + \theta_1 b_{l-1} = 0. \tag{4.32}$$

. This equation can also be written as a determinant of an infinite matrix

$$\Delta(\mu) = \begin{vmatrix} \ddots & \vdots & \vdots & \vdots & \iddots \\ \cdots & (i\mu+2)^2 - \theta_0 & -\theta_1 & 0 & \cdots \\ \cdots & -\theta_1 & i\mu^2 - \theta_0 & -\theta_1 & \cdots \\ \cdots & 0 & -\theta_1 & (i\mu-2)^2 - \theta_0 & \cdots \\ \iddots & \vdots & \vdots & \vdots & \ddots \end{vmatrix} = 0 \tag{4.33}$$

Whittaker and Watson have shown that [33]

$$\Delta(i\mu) = \Delta(0) - \frac{\sin^2(\pi i\mu/2)}{\sin^2(\pi\sqrt{\theta_0}/2)}, \tag{4.34}$$

and therefore, the roots of the determinant (4.33) are given by the roots of the equation

$$\sin^2(\pi i\mu/2) = \Delta(0)\sin^2\left(\pi\sqrt{\theta_0}/2\right). \tag{4.35}$$

Using the identity $\sin^2(x/2) = [1-\cos(x)]/2$, we can then express the Floquet exponent by

$$\mu = \frac{1}{i\pi}\arccos\left[1 - 2\Delta(0)\sin^2\left(\pi\sqrt{\theta_0}/2\right)\right]. \tag{4.36}$$

The right hand side only depends on the system parameters θ_0 and θ_1. The infinite determinant $\Delta(0)$ can be approximated by a sufficiently large finite matrix and therefore, we can compute the Floquet exponents. The Mathieu system is asymptotically stable for the given parameters, when all real parts of the exponents are smaller than zero.

4.3.2 The Damped Mathieu Equation

A generalization of the Mathieu equation can be obtained by adding a damping term to (4.30)

$$\ddot{x} + 2\xi\dot{x} + [\theta_0 + 2\theta_1\cos(2t)]x = 0, \tag{4.37}$$

where $\xi > 0$ is a damping parameter. Substituting $y = e^{\xi t}x$ yields

$$\ddot{y} + [\theta_0 - \xi^2 + 2\theta_1\cos(2t)]y = 0, \tag{4.38}$$

which is an undamped Mathieu equation of the form (4.30). From Theorem 4.2.2 we know that solutions of (4.38) can be written in the form $y(t) = e^{\mu t}p(t)$. The solutions of (4.37) are then given by

$$x(t) = e^{(\xi+\mu)t}p(t). \tag{4.39}$$

Thus, the damped Mathieu equation (4.37) uniformly asymptotically stable if

$$Re(\mu) + \xi < 0. \tag{4.40}$$

The Floquet exponent μ of the undamped Mathieu equation (4.38) can be computed numerically as outlined in the previous section.

Chapter 5

The Damped Pendulum with Torque

In this chapter we will analyze the asymptotic dynamic states of the damped pendulum with constant torque

$$\ddot{\phi} + \alpha\dot{\phi} + K\sin(\phi) = P. \tag{5.1}$$

This system possesses two asymptotic states, a fixed point and a limit cycle. It has been shown, that there exist certain parameter regimes where either only one of these states is stable or both coexist. The phase boundary between the coexistence regime and the globally stable fixed point regime corresponds to a homoclinic bifurcation. We introduce a linearization approach for approximating this boundary. This approach will be generalized to arbitrary network structures in the following chapter. At first, we start with an analysis of the two node system and show how the dynamics of this system is related to (5.1).

5.1 The Two Node System

The most simple network system, consists of a generator and a consumer connected by a single line. The swing equation for this system is given by

$$\ddot{\phi}_1 = P_1 - \alpha\dot{\phi}_1 - K\sin(\phi_1 - \phi_2) \tag{5.2}$$

$$\ddot{\phi}_2 = P_2 - \alpha\dot{\phi}_2 - K\sin(\phi_2 - \phi_1). \tag{5.3}$$

Similar to the damped pendulum with torque, this system has two possible asymptotic states: Either the two nodes are synchronized at a certain frequency or they are desynchronized and oscillating around their natural frequency. Because of the symmetries discussed in Section (3.2) the dynamics of the 4-dimensional system can be reduced to a 2-dimensional system. It turns out that this reduced system can be mapped to the equation of the damped pendulum with torque (5.1). Here, the synchronous and non-synchronous state of the two node system correspond to the stable fixed point and the stable limit cycle of the damped pendulum with torque.

5.1.1 Stability of Fixed Points in the Two Node System

The two node system possesses two different fixed points. We will analyze the linear stability of these points by applying the results of Section 3.3. We assume to be in

the co-rotating frame and therefore $P_1 = -P_2 \equiv P$. The power flow of the system is given by

$$P = K \sin(\phi_1 - \phi_2). \tag{5.4}$$

If we choose $\phi_2 = 0$, the solution of the power flow is given by $\phi_1 = \arcsin(P/K)$, with $|\phi_1 - \phi_2| < \pi/2$. The Laplacian defined as in (3.19) is given by

$$L = \sqrt{K^2 - P^2} \begin{pmatrix} -1 & +1 \\ +1 & -1 \end{pmatrix}. \tag{5.5}$$

Here, we used the relation $\cos(\arcsin(x)) = \sqrt{1 - x^2}$. The eigenvalues of L are $\lambda_1 = 0$ and $\lambda_2 = -2\sqrt{K^2 - P^2}$. The eigenvalues of the Jacobian as defined in (3.29) are then given by

$$\begin{aligned} \sigma_1 &= 0 \\ \sigma_2 &= -\alpha \\ \sigma_3 &= \frac{-\alpha + \sqrt{\alpha^2 - 8\sqrt{K^2 - P^2}}}{2} \\ \sigma_4 &= \frac{-\alpha - \sqrt{\alpha^2 - 8\sqrt{K^2 - P^2}}}{2}. \end{aligned}$$

The eigenvalues σ_1 and σ_2 correspond to the global shift of phases and the global shift of frequencies, which declines exponentially. The eigenvalues σ_3 and σ_4 can be complex numbers and correspond to the damped harmonic eigenmode of the system in opposite rotation directions. For

$$\alpha^2 \geq 8\sqrt{K^2 - P^2} \tag{5.6}$$

these modes are over-damped.

5.1.2 Dimension Reduction of Two Node System

If we make a coordinate change to $\phi_+ = \phi_1 + \phi_2$ and $\phi_- = \phi_1 - \phi_2$, the differential equations decouple and we get

$$\ddot{\phi}_+ = -\alpha \dot{\phi}_+ \tag{5.7}$$

$$\ddot{\phi}_- = 2P - \alpha \dot{\phi}_- - 2K \sin(\phi_-). \tag{5.8}$$

Thus ϕ_+ declines exponentially and the remaining system reduces to a 2-dimensional system. Setting $\phi = \phi_-$, $P' = 2P$ and $K' = 2K$, equation (5.8) becomes

$$\ddot{\phi} = P' - \alpha \dot{\phi} - K' \sin(\phi), \tag{5.9}$$

which is exactly the dynamics of the damped pendulum with torque (5.1). The power flow at the fixed point is given by

$$P' = K' \sin(\phi^*). \tag{5.10}$$

This equation has the two solutions $\phi^* = \arcsin(P'/K')$ and $\phi_2^* = \arcsin(P'/K') + \pi$. We will see that those correspond to a stable fixed point and a saddle point. Assume

a small deviation from the fixed point solution $\phi = \phi^* + \delta\phi$. Then we can expand the sine function and get

$$\delta\ddot{\phi} = -\alpha\delta\dot{\phi} - \sqrt{K'^2 - P'^2}\delta\phi. \tag{5.11}$$

The eigenvalues of the Jacobian are

$$\sigma_+ = \frac{-\alpha + \sqrt{\alpha^2 - 4\sqrt{K'^2 - P'^2}}}{2}$$
$$\sigma_- = \frac{-\alpha - \sqrt{\alpha^2 - 4\sqrt{K'^2 - P'^2}}}{2},$$

and correspond to the eigenvalues σ_3 and σ_4 of the two node system derived in the previous section. A linearization at the other fixed points yields a similar dynamical equation

$$\delta\ddot{\phi} = -\alpha\delta\dot{\phi} + \sqrt{K'^2 - P'^2}\delta\phi, \tag{5.12}$$

with a change of sign in front of the second term on the right hand side. However, this completely changes the dynamical behavior since the eigenvalues of the Jacobian are given by

$$\sigma_+ = \frac{-\alpha + \sqrt{\alpha^2 + 4\sqrt{K'^2 - P'^2}}}{2}$$
$$\sigma_- = \frac{-\alpha - \sqrt{\alpha^2 + 4\sqrt{K'^2 - P'^2}}}{2},$$

and thus, $\sigma_+ > 0$. The fixed point $\phi_2^* = \arcsin(P'/K') + \pi$ is therefore a saddle point of the dynamical system.

5.2 Limit Cycle of the Damped Pendulum with Torque

In this section we will derive different approximations for the limit cycle trajectory and its stability. A low damping approximation $\alpha \ll 1$ of the homoclinic bifurcation between the regime where the stable fixed point is globally asymptotically stable and the regime where stable fixed point and stable limit cycle coexist follows the approach in [16]. An approximation of the limit cycle trajectory for the parameter regime where $(P/\alpha)^2 \gg K$ was derived in [17]. We will assess the stability in this regime by a linearization approach.

5.2.1 Homoclinic Bifurcation Approximation

In the limit of small damping and small torque (5.1) reduces to the dynamics of the nonlinear pendulum

$$\ddot{\phi} + K\sin(\phi) = 0. \tag{5.13}$$

This equation has two fixed points: A stable fixed point $\phi(t) = 0$ and a saddle point $\phi(t) = \pm\pi$. Multiplying (5.13) by $\dot{\phi}$ yields

$$\ddot{\phi}\dot{\phi} + K\sin(\phi)\dot{\phi} = 0, \tag{5.14}$$

which can also be written as

$$\frac{d}{dt}\left[\frac{1}{2}\dot{\phi}^2 - K\cos(\phi)\right] = 0. \tag{5.15}$$

This equation corresponds to the conservation of energy and thus we can define an energy function as

$$E = \frac{1}{2}\dot{\phi}^2 + K\left(1 - \cos(\phi)\right), \tag{5.16}$$

where we assumed that the energy at the stable fixed point is zero, $E(\phi = 0, \dot{\phi} = 0) = 0$. The energy at the saddle point is then $E(\phi = \pm\pi, \dot{\phi} = 0) = 2K$.

In the following we want to evaluate this energy function for the dynamics of the damped pendulum with torque (5.1). The change of energy is given by

$$\frac{dE}{dt} = \ddot{\phi}\dot{\phi} + K\sin(\phi)\dot{\phi} = P\dot{\phi} - \alpha\dot{\phi}^2. \tag{5.17}$$

When the stable fixed point is globally stable, the trajectory in the phase space is spiraling towards the fixed point and the average energy over one period of this spiral is decreasing for all time. However, at the boundary between the globally stable and the coexistence regime there exists a homoclinic orbit that connects the saddle point with itself and the average energy over a period is given by

$$\overline{\frac{dE}{dt}} = 0, \tag{5.18}$$

and therefore

$$P\overline{\dot{\phi}} - \alpha\overline{\dot{\phi}^2} = 0. \tag{5.19}$$

Calculating the time averages $\overline{\dot{\phi}}$ and $\overline{\dot{\phi}^2}$ yields

$$\overline{\dot{\phi}} = \frac{1}{T}\int_0^T \dot{\phi}dt = \frac{1}{T}\int_{-\pi}^{\pi} d\phi = \frac{2\pi}{T} \tag{5.20}$$

$$\overline{\dot{\phi}^2} = \frac{1}{T}\int_0^T \dot{\phi}^2 dt = \frac{1}{T}\int_{-\pi}^{\pi} \dot{\phi}d\phi \tag{5.21}$$

$$= \frac{1}{T}\int_{-\pi}^{\pi} \sqrt{2E(\phi,\dot{\phi}) + 2K(\cos(\phi) - 1)}d\phi. \tag{5.22}$$

For the specific parameters when the fixed point looses global stability and the limit cycle becomes stable there exists a homoclinic orbit that connects the saddle point with itself. With the low damping approximation we can assume assume the energy to be constant throughout the period. Evaluating the integral (5.22) with $E(\phi, \dot{\phi}) \approx 2K$ yields

$$\int_{-\pi}^{\pi} \sqrt{2K + 2K\cos(\phi)}d\phi = 8\sqrt{K}. \tag{5.23}$$

Inserting (5.20), (5.22) and (5.23) into (5.19) finally gives the low-damping approximation of the boundary between the globally stable and the coexistence regime

$$\frac{P}{\alpha} \approx \frac{4}{\pi}\sqrt{K}. \tag{5.24}$$

5.2.2 Linearization Approximation

When the parameter $K = 0$, the dynamics of (5.1) reduces to

$$\ddot{\phi} = P - \alpha\dot{\phi}. \tag{5.25}$$

The dynamics of the frequency $\omega = \dot{\phi}$ is then given by

$$\omega(t) = Ce^{-\alpha t} + \frac{P}{\alpha}. \tag{5.26}$$

Therefore, the model has a stable limit cycle at $\omega = \frac{P}{\alpha}$. For $K > 0$ we assume that the phase can still be approximated by $\phi \approx (P/\alpha)t$ and the frequency is given by $\omega(t) = \frac{P}{\alpha} + f(t)$. Inserting this into (5.1) yields

$$\dot{f} = -\alpha f - K \sin\left(\frac{P}{\alpha}t\right). \tag{5.27}$$

The solution of this differential equation is given by

$$f(t) = \frac{K\alpha}{P^2 + \alpha^4}\left[P\cos\left(\frac{P}{\alpha}t\right) - \alpha^2 \sin\left(\frac{P}{\alpha}t\right)\right] + Ce^{-\alpha t}. \tag{5.28}$$

For $P \gg \alpha^2$ this can be approximated by

$$f(t) \approx \frac{K\alpha}{P}\cos\left(\frac{P}{\alpha}t\right) + Ce^{-\alpha t}, \tag{5.29}$$

and thus the model has a stable limit cycle that is approximately given by

$$\omega(t) \approx \frac{P}{\alpha} + \frac{K\alpha}{P}\cos\left(\frac{P}{\alpha}t\right). \tag{5.30}$$

Integrating this equation yields

$$\phi(t) = \frac{P}{\alpha}t + \frac{K\alpha^2}{P^2}\sin\left(\frac{P}{\alpha}t\right). \tag{5.31}$$

Hence, the initial assumption $\phi \approx (P/\alpha)t$ holds if $(P/\alpha)^2 \gg K$.

We want to generalize this approach for a finite time-dependent variation of the phase

$$\phi(t) = \frac{P}{\alpha}t + \delta\phi(t). \tag{5.32}$$

Inserting this into equation (5.1) yields

$$\delta\ddot{\phi} = -\alpha\delta\dot{\phi} - K\sin\left(\frac{P}{\alpha}t + \delta\phi\right). \tag{5.33}$$

If we assume $\delta\phi$ to be small, we can expand (5.33) to linear order and get

$$\delta\ddot{\phi} \approx -\alpha\delta\dot{\phi} - K\sin\left(\frac{P}{\alpha}t\right) - K\cos\left(\frac{P}{\alpha}t\right)\delta\phi. \tag{5.34}$$

From theorem 4.1.5 we know that this non-homogeneous equation is bounded if the homogeneous equation

$$\delta\ddot{\phi} + \alpha\delta\dot{\phi} + K\cos\left(\frac{P}{\alpha}t\right)\delta\phi = 0 \tag{5.35}$$

is uniformly asymptotically stable. The homogeneous equation (5.35) has the form of a damped Mathieu equation. Therefore, we can determine the the stability as described in Section 4.3.2. The linear approximation of the phase boundary between the regime where the fixed point is globally stable and the regime where fixed point and limit cycle coexist is depicted in Figure 5.1. Although for larger values of K this approximation seems to be inferior compared to the approximation derived in the previous chapter, it still gives a rather convenient result.

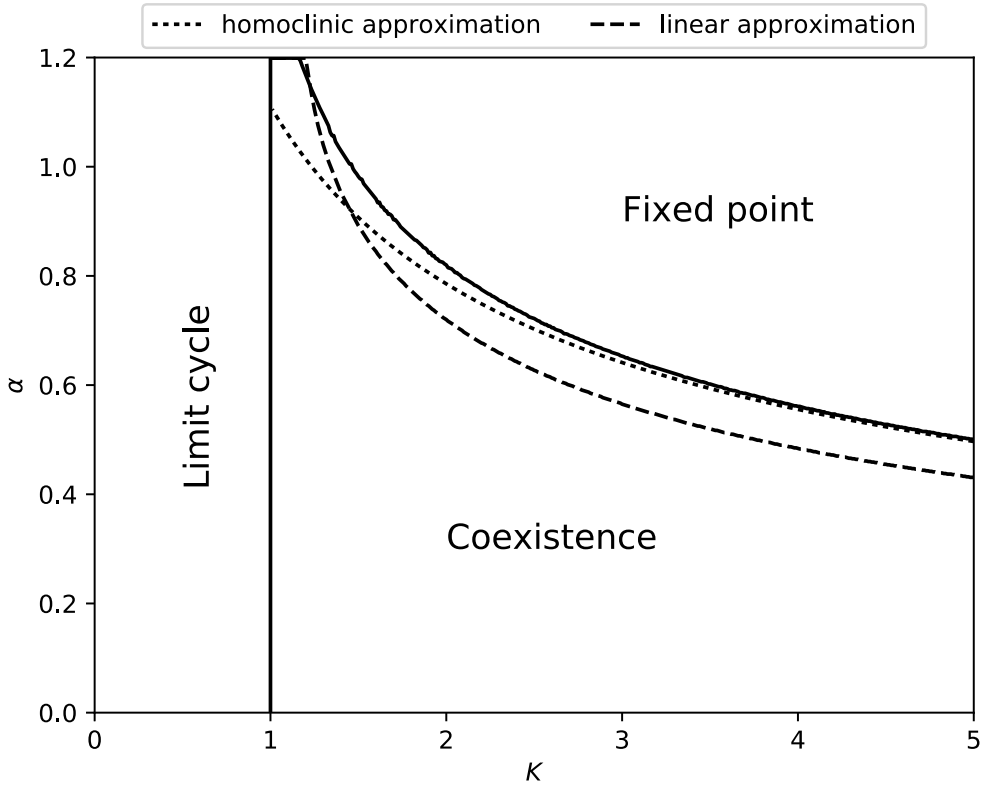

Figure 5.1: Phase boundary in the stability phase diagram of the damped pendulum with torque. The torque parameter is set to $P = 1$. The boundaries are given by the solid lines. The dashed line is the linear approximation of the boundary based on the numerical computation of the Floquet exponents for the corresponding Mathieu equation. The dotted line is the approximation given by equation (5.24).

5.3 The Infinite Grid Model

The dynamics of the damped pendulum with torque is often used as a model of a single generator coupled with strength to a grid. Here, it is assumed that the dynamics of the generator has no influence on the dynamics of the grid. This is equivalent to the assumption that the grid has infinitely large inertia, which is why the model is also known as the *infinite grid model*. The phase angle ϕ_0 of the single generator is measured relative to the phase angle of the grid ϕ^* and the frequency ω is measured in the co-rotating frame of the grid. The fixed point $\phi_0 = \phi^*$ and $\omega = 0$ corresponds to the synchronization with the grid frequency.

5.3.1 Effective Coupling Strength

In this section we will derive the effective coupling strength of a single node $i = 0$ attached to a synchronized grid of n nodes by an arbitrary number of connections. The dynamics is given by the swing equation

$$\ddot{\phi}_i = P_i - \alpha_i \dot{\phi}_i - \sum_{j=0}^{n} K_{ij} \sin(\phi_i - \phi_j), \quad 0 \leq i \leq n. \tag{5.36}$$

We further assume that the synchronized grid is infinitely heavy, i.e. every node has infinite inertia. In Section 2.2.2, we have shown that

$$P_i = \frac{P_i^{source}}{J_i \Omega}, \quad \alpha_i = \frac{D_i}{J_i \Omega}, \quad K_{ij} = \frac{|V_i||V_j|}{x_{ij} J_i \Omega}, \tag{5.37}$$

and thus, $P_i \to 0$, $\alpha \to 0$ and $K_{ij} \to 0$ for $J_i \to \infty$. When we are in the co-rotating frame of the grid, the solutions ϕ_j for $j = 1, \ldots, n$ are simply given by constant phase angles ϕ_j^*. We assume the grid to be in synchronous state and thus

$$P_i = \sum_{j=1}^{n} K_{ij} \sin(\phi_i^* - \phi_j^*) \quad \text{for } j = 1, \ldots, n. \tag{5.38}$$

The dynamics of the system then reduces to the dynamics of the attached node

$$\dot{\phi}_0 = \omega_0 \tag{5.39}$$

$$\dot{\omega}_0 = P_0 - \alpha\omega_0 - \sum_{j=1}^{n} K_{0j} \sin(\phi_0 - \phi_j^*). \tag{5.40}$$

The goal is now to reduce this system to an infinite grid model of the form

$$\ddot{\phi}_0 = P_0 - \alpha\dot{\phi}_0 - K \sin(\phi - \phi^*), \tag{5.41}$$

where K is the effective coupling strength between the single node and the grid and ϕ_* is the effective phase angle of the grid. We can rewrite the sum of coupling terms in (5.40) as

$$\sum_{j=1}^{n} K_{0j} \sin(\phi_0 - \phi_j^*) = \sum_{j=1}^{n} K_{0j} \Im\left[e^{i(\phi_0 - \phi_j^*)}\right] \tag{5.42}$$

$$= \Im\left[e^{i\phi_0} \sum_{j=1}^{n} K_{0j} e^{-i\phi_j^*}\right] \tag{5.43}$$

$$= \Im\left[e^{i\phi_0} \left(\sum_{j=1}^{n} K_{0j} \cos(\phi_j^*) - i \sum_{j=1}^{n} K_{0j} \sin(\phi_j^*)\right)\right]. \tag{5.44}$$

The same can be done for the coupling term in (5.41)

$$K \sin(\phi - \phi^*) = \Im\left[e^{i\phi_0}(K e^{-i\phi^*})\right]. \tag{5.45}$$

Comparing (5.44) and (5.45) we get the relation

$$K e^{i\phi^*} = \sum_{j=1}^{n} K_{0j} \cos(\phi_j^*) + i \sum_{j=1}^{n} K_{0j} \sin(\phi_j^*). \tag{5.46}$$

The absolute of a complex number is given by $|x| = \sqrt{\Re(x)^2 + \Im(x)^2}$ and therefore, the effective coupling strength is given by

$$K = \sqrt{\left(\sum_{j=1}^{n} K_{0j}\cos(\phi_j^*)\right)^2 + \left(\sum_{j=1}^{n} K_{0j}\sin(\phi_j^*)\right)^2} \tag{5.47}$$

$$= \sqrt{\sum_{j,l=1}^{n} K_{0j}K_{0l}\cos(\phi_j^*)\cos(\phi_l^*) + \sum_{j,l=1}^{n} K_{0j}K_{0l}\sin(\phi_j^*)\sin(\phi_l^*)} \tag{5.48}$$

$$= \sqrt{\sum_{j,l=1}^{n} K_{0j}K_{0l}\cos(\phi_j^* - \phi_l^*)}. \tag{5.49}$$

If the node 0 is connected to only one single node j in grid by a link with coupling strength K_{ij}, then (5.49) reduces to $K = K_{0j}$.

5.3.2 Limit Cycle Stability in the Infinite Grid Model

In Section 5.2.1 we derived a low-damping approximation for the boundary between the parameter regime where the stable fixed point is globally stable and the regime, where fixed point and limit cycle coexist. Together with the effective coupling strength (5.49) derived in the previous section we get a condition for the stability of the limit cycle in the infinite grid model that solely depends on the local parameters of the detached node and the solution of the static power flow equations in the grid. With this, the limit cycle is stable if

$$\frac{P_0}{\alpha_0} > \frac{4}{\pi}\left(\sum_{j,l=1}^{n} K_{0j}K_{0l}\cos(\phi_j^* - \phi_l^*)\right)^{\frac{1}{4}}, \tag{5.50}$$

As discussed in Section 3.4.1, in networks of Kuramoto oscillators with inertia we can categorize the nodes into three different classes: nodes with poor, with fair and with high single node basin stability. It has been motivated, that for nodes with fair basin stability the only non-synchronous state that can be induced by a perturbation is the limit cycle state where only the perturbed node is desynchronized from the rest of the grid [17]. For nodes with high single node basin stability this limit cycle is unstable. As a result, equation (5.50) can be interpreted as an approximative condition that a node in a network of Kuramoto oscillators with inertia has high single node basin stability.

Chapter 6

Stability of Synchonous Clusters with Distinct Frequency

In this chapter we will analyze the stability of synchronous clusters in networks of Kuramoto oscillators with inertia. The nonlinear interaction between the oscillators then divides into interactions within the cluster and interactions between the clusters

$$\ddot{\phi}_i = P_i - \alpha_i \dot{\phi}_i - \sum_{j \in \mathcal{C}(i)} K_{ij} \sin(\phi_i - \phi_j) - \sum_{j \notin \mathcal{C}(i)} K_{ij} \sin(\phi_i - \phi_j), \tag{6.1}$$

where $\mathcal{C}(i)$ is the cluster containing oscillator i. We will derive conditions for an exact dynamical decoupling where all individual clusters are in a completely synchronized and in a stationary state. Further, we will show that these conditions correspond to an additional symmetry in the network. In real world topologies such symmetries usually do not occur. However, if the dynamical coupling between clusters is small enough, the clusters can still coexist in almost synchronous states. The corresponding asymptotic dynamical state of the entire system is a limit cycle where all oscillators of one cluster are bound to a frequency range around the clusters synchronization frequency. Therefore, we can treat the dynamical interaction between such clusters as a perturbation of the synchronous state of the separated clusters and make a stability analysis for the linearized system.

Throughout the chapter we will focus on the partitioning of the network into two clusters. The derived methods can easily be generalized to a higher number of clusters. An example of such a partitioning is shown in figure 6.1.

6.1 Exact Dynamical Decoupling of Clusters

In Chapter 3 we have seen that there exists a synchronous solution of (6.1) with a global frequency. In this section we want to investigate the existence of other stationary states of the system where all single oscillators have constant yet not global frequency. In particular we are interested in stationary states where several synchronized clusters of distinct frequencies exist.

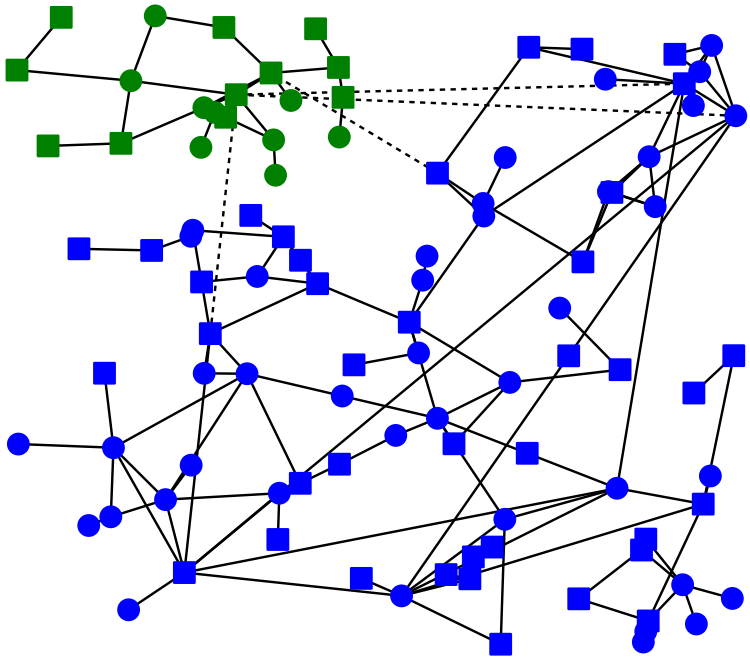

Figure 6.1: Partitioning of a network in two clusters. Power flows on links connecting the clusters (dotted) can be treated as a perturbation of the individual synchronous states.

6.1.1 Stationary States with Non-global Frequencies

When there is no dynamical interaction between the clusters in the network

$$\sum_{j \notin \mathcal{C}(i)} K_{ij} \sin(\phi_i - \phi_j) = 0, \tag{6.2}$$

equation (6.1) reduces to

$$\ddot{\phi}_i = P_i - \alpha_i \dot{\phi}_i - \sum_{j \in \mathcal{C}(i)} K_{ij} \sin(\phi_i - \phi_j). \tag{6.3}$$

This is precisely the swing equation for the subnetwork formed by all nodes and links in cluster $\mathcal{C}$. Thus, there exists a stationary state where all oscillators in the cluster are synchronized with a frequency

$$\omega^*_{\mathcal{C}} = \frac{\sum_{i \in \mathcal{C}} P_i}{\sum_{i \in \mathcal{C}} \alpha_i}. \tag{6.4}$$

The stationary state of the oscillators is then given by

$$\phi_i(t) = \omega^*_{\mathcal{C}(i)} \cdot t + \phi^*_i, \tag{6.5}$$

where the constant phase angles ϕ^*_i are the solutions of the nonlinear power flow equations of the individual clusters

$$P_i - \alpha_i \omega^*_{\mathcal{C}(i)} = \sum_{j \in \mathcal{C}(i)} K_{ij} \sin(\phi^*_i - \phi^*_j). \tag{6.6}$$

Assume the network is partitioned in two clusters $\mathcal{C}_a$ and $\mathcal{C}_b$. For a node $i \in \mathcal{C}_a$, inserting the stationary solutions (6.5) into the decoupling condition (6.2) yields

$$\sum_{j \in \mathcal{C}_b} K_{ij} \sin(\omega_{ab}^* t + \phi_i^* - \phi_j^*) = 0. \tag{6.7}$$

Here we introduced the beat frequency $\omega_{ab}^* = \omega_{\mathcal{C}_a}^* - \omega_{\mathcal{C}_b}^*$. Applying an addition theorem we get

$$\sin(\omega_{ab}^* t) \sum_{j \in \mathcal{C}_b} K_{ij} \cos(\phi_i^* - \phi_j^*) + \cos(\omega_{ab}^* t) \sum_{j \in \mathcal{C}_b} K_{ij} \sin(\phi_i^* - \phi_j^*) = 0, \tag{6.8}$$

and thus for every oscillator i in cluster $\mathcal{C}_a$ the conditions

$$\sum_{j \in \mathcal{C}_b} K_{ij} \cos(\phi_i^* - \phi_j^*) = 0 \tag{6.9}$$

$$\sum_{j \in \mathcal{C}_b} K_{ij} \sin(\phi_i^* - \phi_j^*) = 0 \tag{6.10}$$

have to be fulfilled. If and only if these and the equivalent conditions for the oscillators in cluster $\mathcal{C}_b$ hold, there is no dynamical interaction between the two clusters. Note, that this does not imply there is no power flowing along links connecting both clusters. Actually, the power flow on such a link is given by

$$F_{ij}(t) = K_{ij} \sin(\omega_{ab}^* t + \phi_i^* - \phi_j^*), \tag{6.11}$$

and thus only the temporal mean of this flow vanishes. Further, from (6.7) follows that the sum of all flows between a single oscillator and the opposite cluster must be zero for every point in time.

6.1.2 Symmetries of Decoupled States

In Sections 3.2 and 3.3 we have shown that there exists the symmetry of a homogeneous constant phase shift corresponding to a zero eigenvalue of the Laplacian. It can easily be seen, that there exists a similar symmetry in the case of the exact dynamical decoupling of two clusters corresponding to a homogeneous constant phase shift in only one of the clusters. We will now show, that this symmetry implies an additional zero eigenvalue of the Laplacian. If $\boldsymbol{x}$ is a vector in the null space of L, a similar approach as in equation (2.19) yields

$$0 = \boldsymbol{x}^T L \boldsymbol{x} = \sum_{i,j=1}^{n} K_{ij} \cos(\phi_i^* - \phi_j^*)(x_i - x_j)^2. \tag{6.12}$$

As discussed before, that the vector $\boldsymbol{x} = (1, ..., 1)^T$ obviously fulfills this condition. We will now show, that there exists another linear independent vector that fulfills the condition (6.12) and which can be defined as

$$x_i = \begin{cases} 1 & \text{if } i \in \mathcal{C}_a \\ 0 & \text{if } i \in \mathcal{C}_b. \end{cases} \tag{6.13}$$

With this, we can write (6.12) as

$$0 = \sum_{i=1}^{n} \left(\sum_{j \in \mathcal{C}(i)} K_{ij} \cos(\phi_i^* - \phi_j^*)(x_i - x_j)^2 + \sum_{j \notin \mathcal{C}(i)} K_{ij} \cos(\phi_i^* - \phi_j^*)(x_i - x_j)^2 \right) \tag{6.14}$$

$$= \sum_{i=1}^{n} \sum_{j \notin \mathcal{C}(i)} K_{ij} \cos(\phi_i^* - \phi_j^*). \tag{6.15}$$

In case of exact dynamical decoupling, the condition (6.9) holds and therefore, the vector $\boldsymbol{x}$ defined as in (6.13) is an eigenvector of the Laplacian with corresponding eigenvalue $\lambda_2 = 0$.

Let us now introduce an arbitrary homogeneous phase shift in one cluster

$$\phi_i^* \to \begin{cases} \phi_i^* + \delta & \text{if } i \in \mathcal{C}_a \\ \phi_i^* & \text{if } i \in \mathcal{C}_b. \end{cases} \tag{6.16}$$

Since we assume the coupling K_{ij} to be symmetric and using the fact that cosine is a symmetric function, inserting this into the condition above yields

$$0 = \sum_{i \in \mathcal{C}_a} \sum_{j \in \mathcal{C}_b} K_{ij} \cos(\phi_i^* - \phi_j^* + \delta) \tag{6.17}$$

$$= \sum_{i \in \mathcal{C}_a} \left(\cos(\delta) \sum_{j \in \mathcal{C}_b} K_{ij} \cos(\phi_i^* - \phi_j^*) - \sin(\delta) \sum_{j \in \mathcal{C}_b} K_{ij} \sin(\phi_i^* - \phi_j^*) \right). \tag{6.18}$$

Again, if the conditions (6.9) and (6.10) for exact dynamical decoupling hold, equation (6.18) is fulfilled for any arbitrary phase shift δ. The additional zero eigenvalue of the Laplacian therefore corresponds to a symmetry regarding homogeneous phase shifts in one of the clusters.

When the two cluster do not decouple completely, the additional phase shift symmetry disappears and thus, the eigenvalue $\lambda_2(\delta)$ will depend on the relative phase shift δ between the clusters. Since the clusters are rotating at different speed, the phase shift is in fact permanently changing by $\delta = \omega_{ab}^* t$. Thus, the Laplacian and its eigenvalues become periodically time dependent. The implications of this will be discussed in the following chapter.

6.2 Stability of Almost Decoupled Clusters

The conditions for dynamical decoupling of clusters derived in the previous section are rather strong. Real world networks like power grids usually do not have such highly symmetric structure. However, if the dynamical coupling between different clusters in the network is small enough there exist asymptotically stable solutions close to the synchronous states of the separated clusters. We therefore make an ansatz

$$\phi_i(t) = \omega_{\mathcal{C}(i)}^* \cdot t + \phi_i^* + \delta\phi_i(t), \tag{6.19}$$

where $\omega_{\mathcal{C}(i)}^*$ and ϕ_i^* are the synchronization frequency and the power flow solutions of the cluster $\mathcal{C}(i)$ defined as in (6.4) and (6.6) respectively. If we assume the deviations $\delta\phi_i(t)$ to be small, we can assess the stability of the asymptotic states by linearizing the nonlinear equations and applying the theory of linear time-varying systems introduced in Chapter 4.

6.2.1 Effective Coupling Strength

Assume, the network is again partitioned into two clusters $\mathcal{C}_a$ and $\mathcal{C}_b$. For a node $i \in \mathcal{C}_a$, inserting (6.19) into the coupling term between the clusters yields

$$\sum_{j \in \mathcal{C}_b} K_{ij} \sin(\phi_i - \phi_j) = \sum_{j \in \mathcal{C}_b} K_{ij} \sin(\omega_{ab}^* t + \phi_i^* - \phi_j^* + \delta\phi_i - \delta\phi_j). \tag{6.20}$$

Expanding the sine function to zeroth order we get

$$\sum_{j\in\mathcal{C}_b} K_{ij}\sin(\phi_i-\phi_j) \approx \sum_{j\in\mathcal{C}_b} K_{ij}\sin(\omega^*_{ab}t+\phi^*_i-\phi^*_j). \tag{6.21}$$

Similar to (5.45), we want to define an effective coupling strength K_{ib} for a node $i\in\mathcal{C}_a$ to the cluster $\mathcal{C}_b$ by setting

$$K_{ib}\sin(\omega^*_{ab}t+\phi^*_{ib}) = \sum_{j\in\mathcal{C}_b} K_{ij}\sin(\omega^*_{ab}t+\phi^*_i-\phi^*_j). \tag{6.22}$$

The derivation is then analogous to the one in Section 5.3.1 and yields

$$K_{ib} = \sqrt{\sum_{j,l\in\mathcal{C}_b} K_{ij}K_{il}\cos(\phi^*_j-\phi^*_l)}. \tag{6.23}$$

When the node i is not at the boundary to the other cluster, i.e. there does not exist any link to a node $j\in\mathcal{C}_b$, then $K_{ib}=0$. If there exists exactly one such connection, then $K_{ib}=K_{ij}$. When the conditions (6.9) and (6.10) for dynamical decoupling are fulfilled, then also $K_{ib}=0$. Note, that by definition $K_{ib}\geq 0$. On the other hand, the effective coupling becomes maximal if $\phi^*_j=\phi^*_l$ for all $j,l\in\mathcal{C}_b$ and then

$$K_{ib} = \sqrt{\sum_{j,l\in\mathcal{C}_b} K_{ij}K_{il}} = \sqrt{(\sum_{j,l\in\mathcal{C}_b} K_{ij})^2} = \sum_{j\in\mathcal{C}_b} K_{ij}. \tag{6.24}$$

The effective coupling is thus bounded by

$$0 \leq K_{ib} \leq \sum_{j\in\mathcal{C}_b} K_{ij}. \tag{6.25}$$

Generally, the coupling K_{ib} gets small when the phases ϕ^*_j of the nodes $j\in\mathcal{C}_b$ connected to a node $i\in\mathcal{C}_a$ are widely spread. On the other hand, when the phase differences of all nodes in cluster $\mathcal{C}_b$ that are connected to i fulfill $|\phi^*_j-\phi^*_l|<\pi/2$ then the coupling has a lower bound

$$K_{ib} = \sqrt{\sum_{j\in\mathcal{C}_b} K^2_{ij} + \sum_{j\neq l\in\mathcal{C}_b} K_{ij}K_{il}\cos(\phi^*_j-\phi^*_l)} \geq \sqrt{\sum_{j\in\mathcal{C}_b} K^2_{ij}}. \tag{6.26}$$

In this case, the dynamical coupling to the other cluster only gets small if there are very few connections with small coupling strengths K_{ij}.

6.2.2 Linearization of the Dynamical Equations

In this section we want to linearize the system of nonlinear differential equations (6.1). For this purpose, we insert the ansatz (6.19) and expand the sine functions to first order. For a node $i\in\mathcal{C}_a$ we then get

$$\begin{aligned}\delta\ddot{\phi}_i = &-\alpha_i\delta\dot{\phi}_i + \sum_{j\in\dashv} L^a_{ij}\delta\phi_j - K_{ib}\sin(\omega^*_{ab}t+\phi^*_{ib})\\ &-\sum_{j\in\lfloor} K_{ij}\cos(\omega_{ab}t+\phi^*_{ij})(\delta\phi_i-\delta\phi_j).\end{aligned} \tag{6.27}$$

Here we used the definition of the effective coupling (6.22) and the fact that the phase angles ϕ_i^* of the nodes in $\mathcal{C}_a$ fulfill the power flow equations (6.6). We further introduced the Laplacian of the cluster $\mathcal{C}_a$

$$L_{ij}^a = -\delta_{ij} \sum_{l \in a} K_{il} \cos(\phi_i^* - \phi_l^*) + K_{ij} \cos(\phi_i^* - \phi_j^*). \tag{6.28}$$

For the nodes in cluster $\mathcal{C}_b$ a similar result can be derived. The major difference is a change the sign of the zeroth order term of the expansion due to the definition of ω_{ab} and the fact that the sine is an odd function. By setting $\delta\omega_i = \delta\dot{\phi}_i$ the system of linear ordinary differential equations can be written as a first order system

$$\begin{pmatrix} \delta\dot{\phi} \\ \delta\dot{\omega} \end{pmatrix} = \begin{pmatrix} 0 & 1 \\ L(t) & -\alpha \end{pmatrix} \begin{pmatrix} \delta\phi \\ \delta\omega \end{pmatrix} + \begin{pmatrix} 0 \\ s(t) \end{pmatrix}, \tag{6.29}$$

with $\alpha = \mathrm{diag}(\alpha_i)$, the non-homogeneous coupling

$$s_i(t) = \begin{cases} -K_{ib} \sin(\omega_{ab}^* t + \phi_{ib}^*) & \text{if } i \in \mathcal{C}_a \\ +K_{ia} \sin(\omega_{ab}^* t + \phi_{ia}^*) & \text{if } i \in \mathcal{C}_b, \end{cases} \tag{6.30}$$

and the time dependent Laplacian $L(t) = L^0 + L^1(t)$. Here, L^0 is the Laplacian of the two separated clusters

$$L^0 = \begin{pmatrix} L^a & 0 \\ 0 & L^b \end{pmatrix}, \tag{6.31}$$

and $L^1(t)$ the Laplacian of the 'coupling network' between the two clusters

$$L_{ij}^1(t) = -\delta_{ij} \sum_{l \notin \mathcal{C}(i)} K_{il} \cos(\omega_{ab} t + \phi_{ij}^*) + K_{ij} \cos(\omega_{ab} t + \phi_{ij}^*), \quad j \notin \mathcal{C}(i). \tag{6.32}$$

Equation (6.29) is a non-homogeneous linear periodic system of the form

$$\dot{x} = [A + B(t)]\, x + f(t), \tag{6.33}$$

with the two matrices

$$A = \begin{pmatrix} 0 & 1 \\ L^0 & -\alpha \end{pmatrix}, \quad B(t) = \begin{pmatrix} 0 & 0 \\ L^1(t) & 0 \end{pmatrix}. \tag{6.34}$$

$B(t)$ and $f(t)$ are periodic functions with period $T = 2\pi/\omega_{ab}$.

6.2.3 Analytic Conditions for Linear Stability

From Theorem 4.1.5 follows that (6.33) is bounded if the homogeneous system

$$\dot{x} = [A + B(t)]\, x \tag{6.35}$$

is uniformly asymptotically stable. Further, if the decoupled system

$$\dot{x} = Ax, \tag{6.36}$$

with A defined in (6.34) is uniformly asymptotically stable, i.e. the real parts of all eigenvalues of A are smaller than zero, it follows from theorem 4.1.4 that the system

(6.35) is uniformly asymptotically stable if $\int_{t_0}^{t} |B(s)|ds$ is growing linearly with a rate γ smaller than a certain constant. Applying the spectral norm we get

$$|B(t)|_2 = \sqrt{\lambda_{max}\left(B^T(t)B(t)\right)} = \sqrt{\lambda_{max}\left([L^1(t)]^2\right)}, \tag{6.37}$$

and therefore

$$\int_0^T |B(s)|ds = \int_0^T \sqrt{\lambda_{max}\left([L^1(t)]^2\right)} = \gamma \cdot T, \tag{6.38}$$

where $T = 2\pi/\omega_{ab}$ is the periodicity of $B(t)$.

The fundamental matrix solution of (6.36) is given by $X(t)X^{-1}(t_0) = e^{A(t-t_0)}$. We have shown, that for the decoupled system the Jacobian A has two zero eigenvalues. These correspond to homogeneous phase shifts in each cluster and do not change the dynamics of the system. We can hence set one phase per cluster to zero and thereby reduce the dimension of the dynamical system by two. We further assume, that the two clusters are both in a stable synchronous state and therefore

$$|X(t)X^{-1}(t_0)| = |e^{A(t-t_0)}| \leq e^{-\eta t}, \tag{6.39}$$

where

$$\eta = \min_i |\Re[\lambda_i(A)]| \tag{6.40}$$

is the slowest decline rate of the decoupled system (6.36). From (4.17) it follows, that the homogeneous system (6.35) is uniformly asymptotically stable and thus, the non-homogeneous system is bounded if $\gamma < \eta$ or

$$\frac{1}{T}\int_0^T \sqrt{\lambda_{max}\left([L^1(t)]^2\right)} < \min_i |\Re[\lambda_i(A)]|. \tag{6.41}$$

The inhomogeneity $f(t)$ is bounded by

$$|f(t)|_2 = \sqrt{\sum_i |f_i(t)|^2} \leq \sqrt{\sum_{i\in\mathcal{C}_a} K_{ib}^2 + \sum_{i\in\mathcal{C}_b} K_{ia}^2}. \tag{6.42}$$

From (4.20) it follows that the asymptotic solution of the non-homogeneous system is bounded by

$$|x(t)|_2 \leq \frac{1}{\eta}\sqrt{\sum_{i\in\mathcal{C}_a} K_{ib}^2 + \sum_{i\in\mathcal{C}_b} K_{ia}^2}. \tag{6.43}$$

6.2.4 Numeric Approach for Determining Stability

In this section we are going to outline an approach for determining the stability of the linearized system (6.29) numerically. From Theorem 4.1.5 follows that the system is bounded if the homogeneous system 6.35 is uniformly asymptotically stable. The idea is now to determine the stability of the homogeneous system by using the Floquet theory introduced in Section 4.2. From theorem 4.2.3 follows that a homogeneous linear periodic system is uniformly asymptotically stable if all Floquet exponents have negative real part. We can determine the Floquet exponents of the system by a numerical integration of the system over one period $T = 2\pi/\omega_{ab}$ as outlined in Section 4.2.

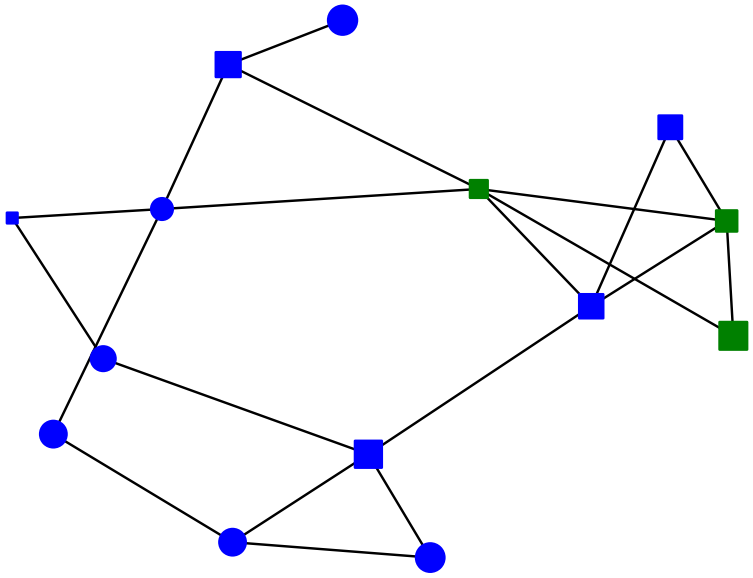

Figure 6.2: Cluster stability in the IEEE 14-bus system. The power inputs P_i are drawn from a bimodal distribution that is given by a sum of two normal distributions with mean $\mu = +1$ and $\mu = -1$ and variance $\sigma = 0.4$. Generators ($P_i > 0$) are represented as squares and consumers ($P_i < 0$) are represented as circles. The node size is proportional to $|P_i|$.

We will now demonstrate the approach for the example of a three node cluster in the IEEE 14-bus system (Figure 6.2). As seen above, the stability of the linearized system is very sensible to the power flows in the different clusters. Therefore, we want to identify certain distributions of power inputs for which the clustered state is stable. For this purpose, we randomly draw power inputs P_i from a bimodal distribution that is given by a sum of two normal distributions centered around $+1$ and -1 and calculate the nonlinear power flow. For every power flow scenario in the network we integrate the linearized system over one period and determine the Floquet exponents. In this manner, we can identify the scenarios where the linearized system (6.29) is bounded. Finally, we verify the stability of the clustered state in the nonlinear system by a numerical integration with the initial conditions of the synchronous states in the separated clusters and by switching on the coupling between the clusters at $t = 0$. The limit cycle of such an asymptotically stable state is shown in Figure 6.3.

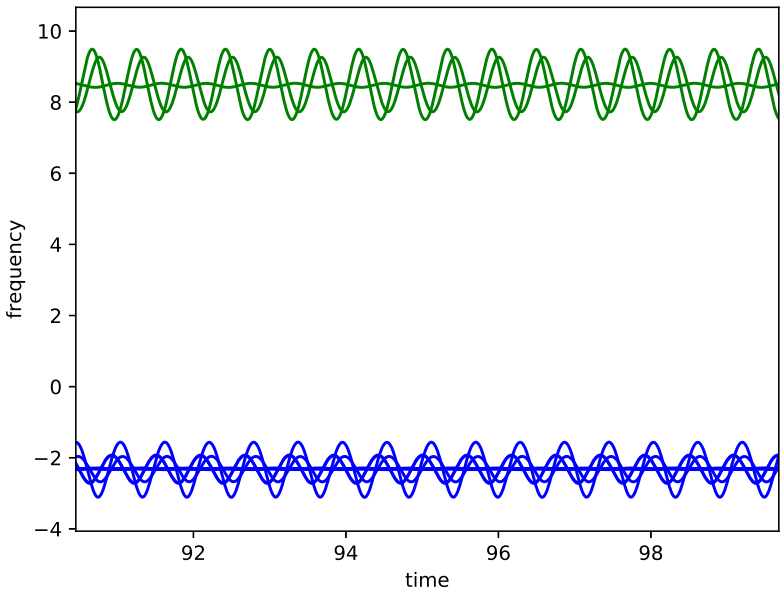

Figure 6.3: Limit cycle of the clustered state in the nonlinear system. The distribution of the power inputs is the one shown in Figure 6.2. The damping and coupling parameters $\alpha = 0.1$ and $K = 4$ are homogeneous in the network. The maximal real part of all Floquet exponents of the linearized system is $\lambda_{max} = -0.042$.

Chapter 7

Tri-Stability of Sprout Nodes

In the previous chapters we have shown that in networks of Kuramoto oscillators with inertia there may exist certain asymptotically stable limit cycles. All of these solutions follow a similar pattern: single oscillators or clusters of oscillators are desynchronized from the rest of the grid and oscillate around their natural frequency or the internal synchronization frequency of the cluster. In this chapter we will show that for a certain type of nodes, so-called *sprout nodes*, there may exist an additional limit cycle where the single node is desynchronized from the rest of the grid and oscillates around a frequency that lies in between of the global synchronization frequency and the natural frequency of the node. Analogous to the infinite grid model introduced in Section 5.3.2 that reproduces the possible asymptotic states of single nodes, we are going to derive a low-dimensional model that reproduces different limit cycles of sprout nodes.

7.1 Topological Classification of Nodes

With the help of the probabilistic stability measures outlined in Section 3.4 it has been shown that the local network structure has a significant impact on the stability of single nodes [17, 29, 22]. In particular, tree-like structures are significantly larger vulnerability to local perturbations [17]. Therefore, a more detailed classification of nodes in such structures was introduced in [22].

A subgraph of a graph $\mathcal{G}$ is called a *tree-shaped part* $\mathcal{T}'$ if it is a tree and is maximal with the property that there is exactly one node $r \in \mathcal{T}$ that has at least one neighbor in $\mathcal{G}' - \mathcal{T}'$. The node r is called the *root* of $\mathcal{T}'$. By definition it has a degree $k(r) \geq 3$. The non-root nodes within tree-like shapes can be divided into *leave nodes* l that have degree $k(l) = 1$ and inner tree nodes that are located between the root and the leaves. All nodes that are not part of tree-shaped parts are referred to as *bulk nodes* b.

The smallest possible tree-shape part consists of a root and a number of leaves. Such leaves are denoted as *sprout nodes* s. These nodes can be further separated into so-called *dense sprouts* having high degree ($k(s) \geq 6$) and *sparse sprouts* having low degree ($k(s) \leq 5$). In contrast, leaves of larger tree-shaped parts are referred to as *proper leaves*. The classification of nodes in an example network is depicted in Figure 7.1.

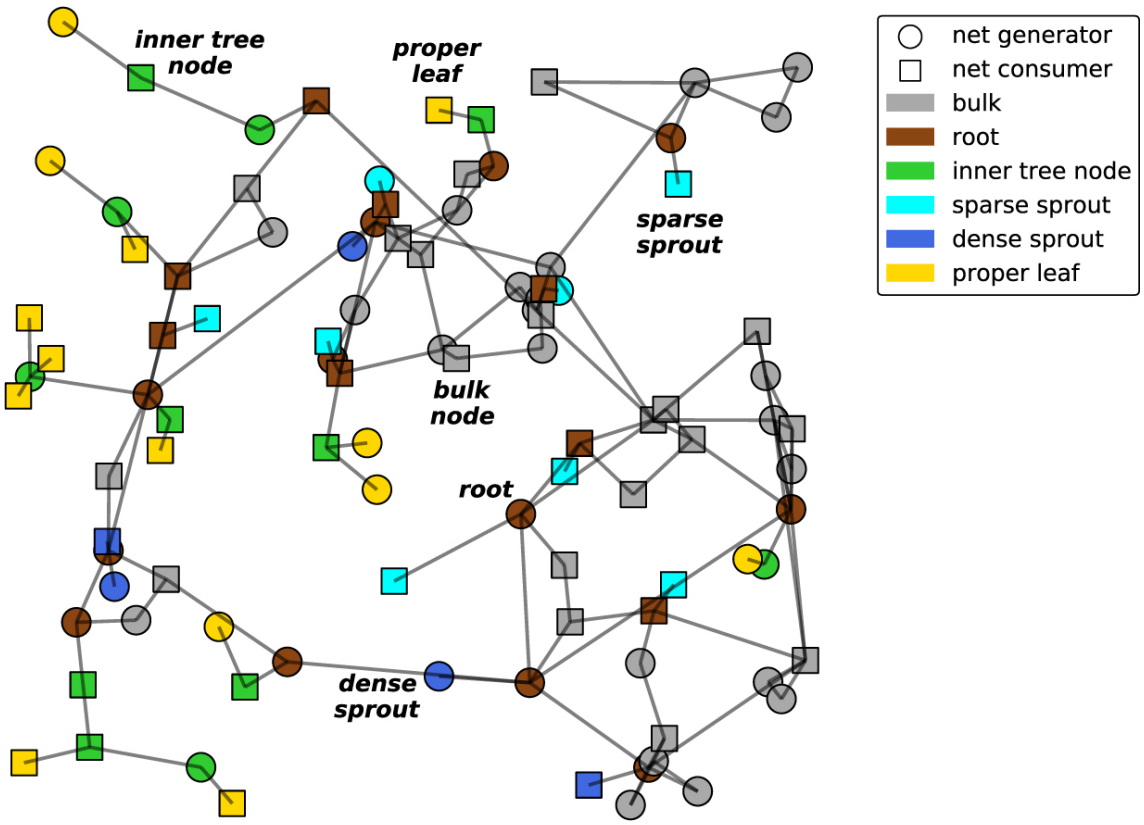

Figure 7.1: Spatially embedded representation of a random synthetic power grid. Nodes are colored according to their topological class. (Figure by Nitzbon et al. (2017) [22] / CC BY 3.0)

Analyzing the dynamics of a large ensemble of networks reveals that the topological properties used in the classification scheme above have indeed a large impact on the transient and asymptotic behavior of the system. Figure 7.2 shows scatter plots of the single node basin stability and single node survivability for different frequency bounds ω^+. It becomes evident that nodes of the same topological class tend to have similar dynamical properties.

7.2 Additional Limit Cycle States of Sprout Nodes

The upper right plot of Figure 7.2 gives a rather astonishing result. The parameters of the swing equation are chosen to $K_i = 8$, $\alpha_i = 0.1$ and $P_i = \pm 1$. The natural frequency of the individual oscillators is therefore $\omega_i' = P_i/\alpha_i = 10$. The frequency bound of the survivability measure is chosen to $\omega^+ = 7.5 < \omega_i'$ and thus, every asymptotic dynamical state with single nodes being desynchronized from the grid should violate the survivability bound. However, in the scatter plot there is a large number of nodes having a larger survivability than basin stability. This means that for a significant number of perturbations at these nodes the system does not return to the global synchronous state but at the same time the trajectories of all nodes stay beneath the bound ω^+.

A possible explanation of this behavior could be that these perturbation lead to a state of synchronized clusters with all frequencies being smaller than ω^+. However,

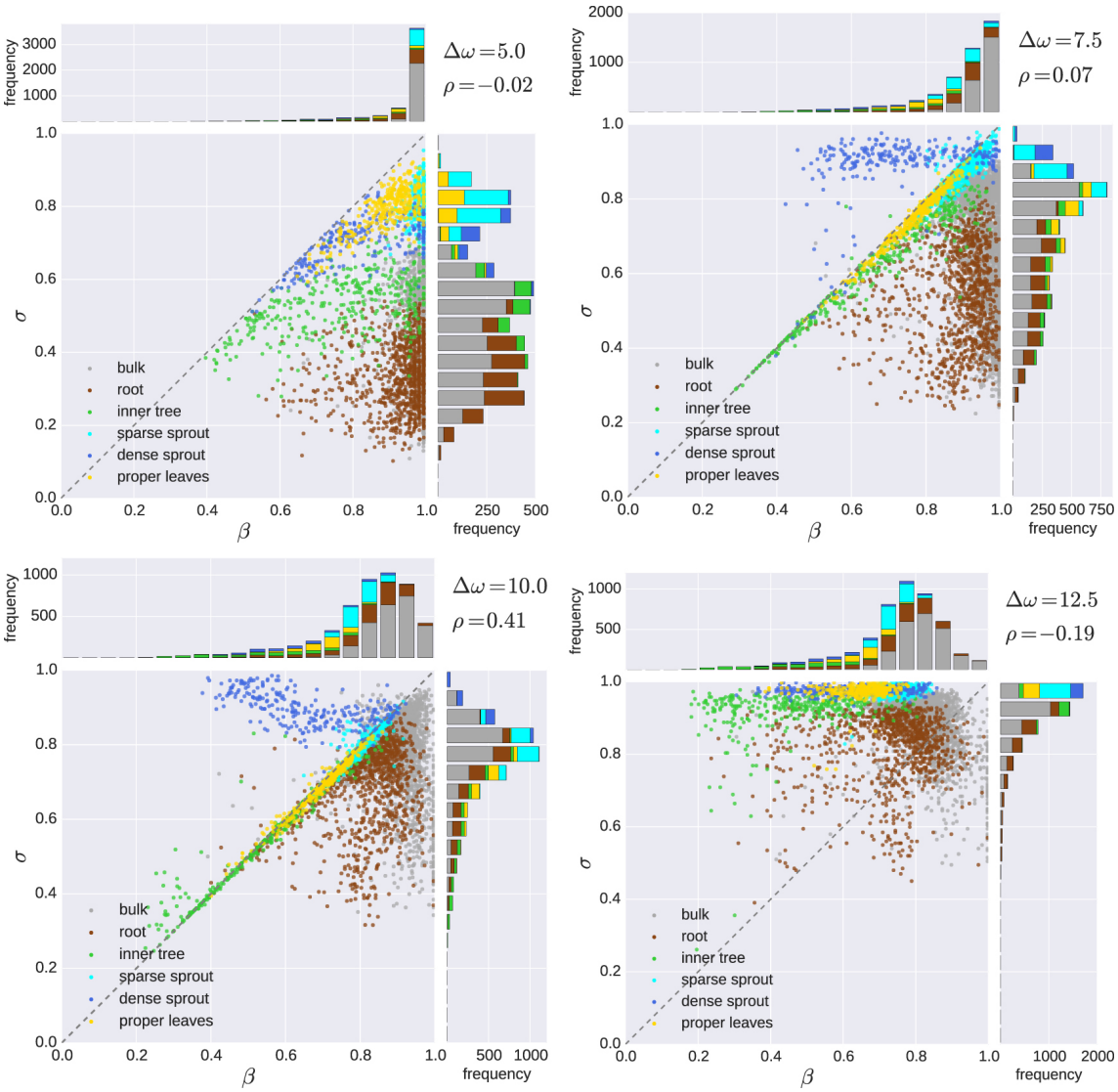

Figure 7.2: Scatter plots and distributions of single-node basin stabilities and survivabilities for an ensemble of 50 randomly generated networks with $n = 100$ nodes each. The nodes are colored corresponding to their topological class. Each of the four plots has a different perturbation level $\Delta\omega$ and survivability bound $\omega^* = \Delta\omega$. (Figure by Nitzbon et al. (2017) [22] / CC BY 3.0)

an analysis of the trajectories reveals that the asymptotic states are characterized by only a single oscillator being desynchronized from the rest of the grid and oscillating around a frequency that is about half the natural frequency ω_i'. The conclusion is that for these nodes there exists an additional stable limit cycle. Remarkably, almost all nodes showing this specific behavior are sprout nodes, particularly sprout nodes with high degree (dense sprouts). The trajectories for the different asymptotic dynamical states of a sprout note is depicted in Figure 7.3.

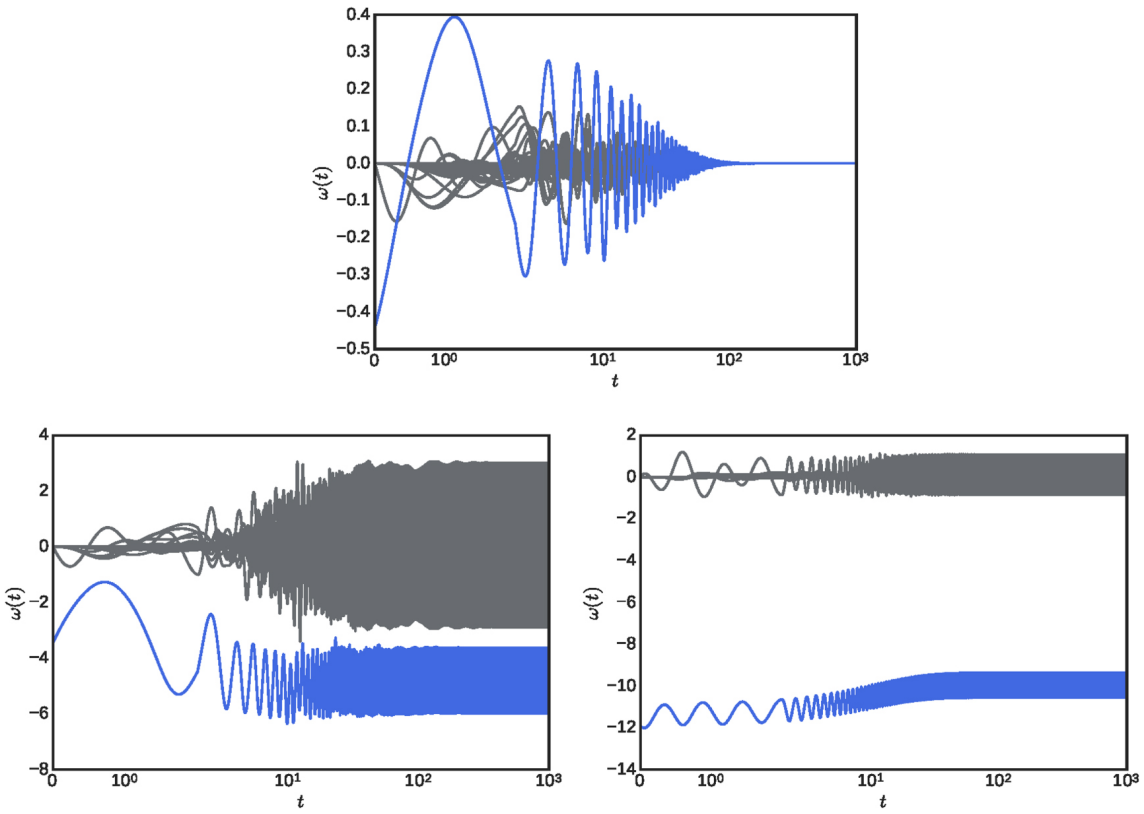

Figure 7.3: Asymptotic dynamical states of a sprout node. In the upper plot the system converges towards the global synchronous state. The lower plots show the two distinct limit cycle states of the sprout node. (Figure by Nitzbon et al. (2017) [22] / CC BY 3.0)

7.3 Low-dimensional Model of Sprout Node Dynamics

In this section we want to derive a low-dimensional model for the dynamics of sprout nodes that reproduces the different asymptotic states. If we denote the sprout node by s and the root node by r the entire dynamics of the system is given by

$$\ddot{\phi}_s = P_s - \alpha_s \dot{\phi}_s - K_{sr} \sin(\phi_s - \phi_r) \tag{7.1}$$

$$\ddot{\phi}_r = P_r - \alpha_r \dot{\phi}_r - K_{rs} \sin(\phi_r - \phi_s) - \sum_{j \neq s} K_{rj} \sin(\phi_r - \phi_j) \tag{7.2}$$

$$\ddot{\phi}_i = P_i - \alpha_i \dot{\phi}_i - K_{jr} \sin(\phi_i - \phi_r) - \sum_{j \neq r} K_{ij} \sin(\phi_i - \phi_j) \quad \text{for } i \neq s, r. \tag{7.3}$$

We now make a similar approach as in the case of the infinite grid model in Section 5.3.1 and assume that all nodes $i \neq s, r$ have infinite inertia. We further assume that all these nodes are in a synchronous state and that we are in the co-rotating frame of this cluster. The dynamical equations then reduce to

$$\ddot{\phi}_s = P_s - \alpha_s \dot{\phi}_s - K_{sr} \sin(\phi_s - \phi_r) \tag{7.4}$$

$$\ddot{\phi}_r = P_r - \alpha_r \dot{\phi}_r - K_{rs} \sin(\phi_r - \phi_s) - \sum_{j \neq s} K_{rj} \sin(\phi_r - \phi_j^*) \tag{7.5}$$

$$P_i = \sum_{j \neq r} K_{ij} \sin(\phi_i^* - \phi_j^*) \quad \text{for } i \neq s, r. \tag{7.6}$$

Again, we can introduce an effective coupling strength of the root to the rest of the grid given by setting

$$K_{rg}\sin(\phi_r - \phi_g^*) = \sum_{j\neq s} K_{rj}\sin(\phi_r - \phi_j^*). \tag{7.7}$$

The derivation is analogous to the one in Section 5.3.1 and yields

$$K_{rg} = \sqrt{\sum_{j,l\neq s} K_{rj}K_{rl}\cos(\phi_j^* - \phi_l^*)}. \tag{7.8}$$

Inserting this into the dynamical equation of the root node and measuring all phase angles relative to ϕ_g^* finally yields

$$\ddot{\phi}_s = P_s - \alpha_s\dot{\phi}_s - K_{sr}\sin(\phi_s - \phi_r) \tag{7.9}$$

$$\ddot{\phi}_r = P_r - \alpha_r\dot{\phi}_r - K_{rs}\sin(\phi_r - \phi_s) - K_{rg}\sin(\phi_r). \tag{7.10}$$

So with the assumption that the dynamics of root and sprout has no major impact on the dynamics of the rest of the grid we were able to reduce the high-dimensional system to a system of dimension four. The reduced system is nevertheless capable of capturing the tri-stability of the sprout node having a synchronous fixed point solution as well as two stable limit cycle solutions for a certain parameter range as depicted in Figure 7.4.

When the coupling K_{rg} between root and grid goes towards zero, the reduced model turns into the familiar two node system possessing bi-stability as derived in Section 5.1. The coupling K_{rg} is therefore the relevant bifurcation parameter for the transition between bistable and tristable regime. With the reasonable assumption there are no overly large power imbalances and long range connections to the root node the phase angle differences in 7.8 are usually small $|\phi_j^* - \phi_l^*| < \pi/2$. Further, the simulations underlying the scatter plot Figure 7.2 where done with homogeneous coupling $K_{ij} = K$. With this, it follows from equations (6.25) and (6.26) that the effective coupling of the root is bounded by

$$\sqrt{k-1}K \leq K_{rg} \leq (k-1)K, \tag{7.11}$$

where $k = k(r)$ is the degree of the root. Thus, with the assumptions made above the bifurcation parameter is monotonously increasing with the degree of the root. This explains why particularly dense sprouts tend to reveal the previously unexpected dynamical behavior depicted in Figure 7.2.

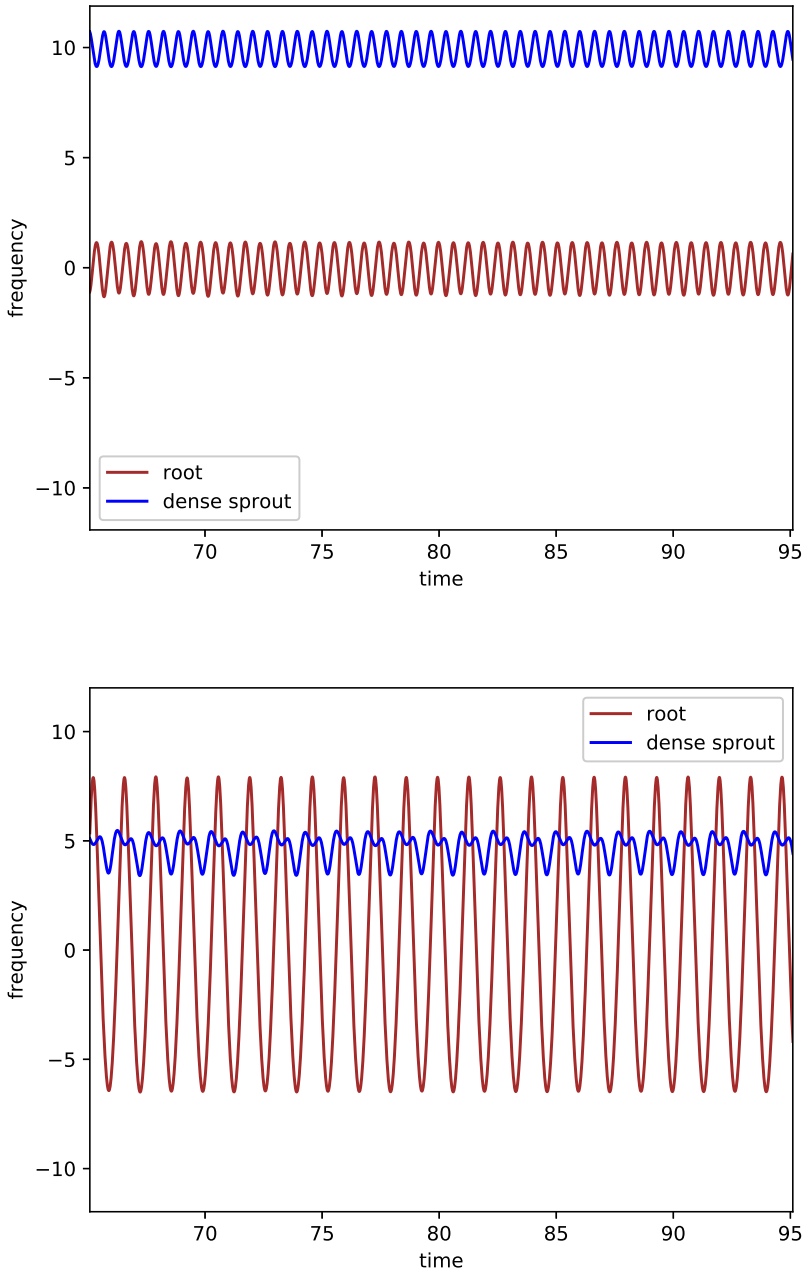

Figure 7.4: The two limit cycles of a sprout node given by a numerical integration of the reduced model (7.9) and (7.10). In the upper plot the sprout is oscillating around its natural frequency $P/\alpha = 10$, whereas in the lower plot it is oscillating around a frequency that is only about half its natural frequency. A trajectory approaching this asymptotic state would not necessarily violate a frequency bound $\omega^+ < P/\alpha$.

Chapter 8

Discussion and Outlook

In Chapter 5 we analyzed the dynamics of the damped pendulum with torque. We have shown that the most simple network of Kuramoto oscillators with inertia, the two node system, can be reduced to this model. The dynamical system possesses two asymptotic states, a fixed point and a limit cycle. There are three different regimes: For $P > K$ only the limit cycle is stable. For $P > K$ either both asymptotic states coexist or the fixed point is globally stable. The phase boundary between those to regimes corresponds to a homoclinic bifurcation. Manik et al. [16] derived a low damping approximation ($\alpha \ll 1$) for this boundary. We propose an alternative approximation for the parameter range $(P/\alpha)^2 \gg K$ by linearizing the dynamics. With this approach we can can translate the problem to a stability analysis of the well-known Mathieu equation. Our approach gives a fair albeit inferior approximation of the phase boundary compared to the low damping approach. The major advantage is however, that it can be easily generalized to higher order systems as the swing equation in a network.

In Section 5.3.1 we derived an effective coupling strength of a single node i to a cluster $\mathcal{C}$ of synchronized oscillators

$$K_{i\mathcal{C}} = \sqrt{\sum_{j,l\in\mathcal{C}} K_{ij}K_{il}\cos(\phi_j^* - \phi_l^*)}. \tag{8.1}$$

This coupling strength is the zeroth order approximation of the coupling from the cluster to the single node and it is exact for the infinite grid limit where the dynamics of the node has no impact on the dynamics of the cluster. The effective coupling may be much smaller than the sum of the individual coupling strengths due to the phase shifts between the single oscillators resulting from the power flow in the cluster. Under specific conditions the coupling may even vanish. A necessary condition is here, that there are pairs of nodes in the cluster having large phase angle differences $|\phi_j^* - \phi_l^*| > \pi/2$ corresponding to large power flows between different parts of the cluster. Note, that the nodes j and l do not necessarily have to be connected. In fact, such large phase differences of adjacent nodes are rather unusual and may even destabilize the cluster itself. Large phase distances are more likely to occur between pairs of nodes that are distant in the network.

By using the effective coupling strength and the low-damping approximation of the phase boundary for the damped pendulum with torque, we were able to derive an analytic condition for the existence of solitary states in the infinite grid

approximation. Solitary states are stable limit cycles where an all but one oscillator are synchronized. With the assumption that the dynamics of single oscillator has no impact on the rest of the grid there exists a solitary state for node i if

$$\omega_i' > \frac{4}{\pi}\sqrt{K_{ig}}, \tag{8.2}$$

where $\omega_i' = P_i/\alpha_i$ is the natural frequency of the single oscillator and K_{ig} is the effective coupling strength to the rest of the grid. Hence, the existence of solitary states does not only depend on the local parameters of the single oscillators but also on the power flow in the network. A next step should be to verify the validity of (8.2) by a numerical simulation of oscillator networks.

Solitary states are a special case of the more general situation that groups of oscillators form almost synchronous clusters that coexist in the network and oscillate with distinct frequencies. In Section 6.1 we have shown that these clusters completely decouple if the effective coupling strength of all nodes to the opposite clusters vanishes. For realistic network topologies we would not expect such a highly symmetric structure but when the dynamical coupling is small enough the may still persist. We made an approach were we treated the coupling as a perturbation of the synchronous states in the separated cluster. Using a linearization approach similar as in the case of the damped driven pendulum we were able to derive a condition for linear stability

$$\frac{\omega_{ab}}{2\pi}\int_0^{2\pi/\omega_{ab}} \sqrt{\lambda_{max}\left([L^1(t)]^2\right)} < \min_i |\Re[\lambda_i(A)]|, \tag{8.3}$$

where ω_{ab} is the beat frequency of the two clusters, A is the Jacobian of the separated clusters and $L^1(t)$ is the Laplacian of the coupling network. This condition is a rather conservative estimate of the linear stability since it does not take into account how the perturbations couple to the modes of the individual clusters. Further research should attempt to improve the approach by taking the network structure into account. However, we have shown, that the linear stability of a specific case can also be determined numerically by computing the Floquet exponents of the linearized system as outlined in Section 6.2.4. This approach is rather efficient, since it avoids time-consuming computation of long transient trajectories.

Note however, that linear stability is neither a necessary nor sufficient condition for the stability of the corresponding state in the nonlinear system. The linearization of the dynamics is only valid if the mutual dynamically interactions between the individual clusters are sufficiently small. The asymptotic states of the nonlinear equation are stable limit cycles and the stability of such periodic orbits can usually be assessed by linearizing around the specific orbit [10]. However, in case of the swing equation we do not know the exact mathematical form of these orbits. Nevertheless, for small dynamical couplings the periodic orbit stays close to the stationary solution of the decoupled case and and we expect a strong correlation between linear and nonlinear stability. This assumption is also supported by the satisfying results for the case of the two node system. Further investigations should verify the validity of the linear approximation also for larger networks.

In Chapter 7 we have shown that for a certain class of nodes, the so-called sprout nodes, there exists an additional solitary state. Following a similar approach as for

the solitary states in the infinite grid approximation, we were able to derive a low-dimensional model that reproduces the tri-stability of these nodes having two stable limit cycles and the synchronous fixed point for a certain parameter regime. We have motivated that the relevant bifurcation parameter for the transition between the bistable and tristable regime is the effective coupling strength between root node the sprout is attached to and the rest of the grid. We explained that for typical network structures and power flows this effective coupling is larger for higher degrees of the root node. Further research should carry out a detailed bifurcation analysis of this system to gain a deeper insight into the nonlinear dynamics of this exotic solitary state which is neither synchronized nor decoupled.

Bibliography

[1] R. Albert and A.-L. Barabási. Statistical mechanics of complex networks. *Reviews of modern physics*, 74(1):47, 2002.

[2] S. Auer, K. Kleis, P. Schultz, J. Kurths, and F. Hellmann. The impact of model detail on power grid resilience measures. *The European Physical Journal Special Topics*, 225(3):609–625, 2016.

[3] S. Boccaletti, V. Latora, Y. Moreno, M. Chavez, and D.-U. Hwang. Complex networks: Structure and dynamics. *Physics reports*, 424(4):175–308, 2006.

[4] C. Chicone. Ordinary differential equations with applications. *Texts in Applied Mathematics*, 34, 2006.

[5] Deutsche Energie-Agentur (dena). Momentanreserve 2030. Bedarf und Erbringung von Momentanreserve 2030. 2016.

[6] ENTSO-E. High penetration of power electronic interfaced power sources. guidance document for national implementation for network codes on grid connection. 2017.

[7] P. Erdös and A. Rényi. On random graphs i. *Publlicationes Mathematicae*, 6:290–297, 1959.

[8] G. Filatrella, A. H. Nielsen, and N. F. Pedersen. Analysis of a power grid using a kuramoto-like model. *The European Physical Journal B-Condensed Matter and Complex Systems*, 61(4):485–491, 2008.

[9] J. J. S. Grainger, W. D. J. J. Grainger, and W. D. Stevenson. *Power system analysis*. 1994.

[10] J. Guckenheimer and P. J. Holmes. *Nonlinear oscillations, dynamical systems, and bifurcations of vector fields*, volume 42. Springer Science & Business Media, 2013.

[11] J. K. Hale. Ordinary differential equations. 1980.

[12] F. Hellmann, P. Schultz, C. Grabow, J. Heitzig, and J. Kurths. Survivability of deterministic dynamical systems. *Scientific reports*, 6:29654, 2016.

[13] G. W. Hill. On the part of the motion of the lunar perigee which is a function of the mean motions of the sun and moon. *Acta mathematica*, 8(1):1–36, 1886.

[14] Y. Kuramoto. Self-entrainment of a population of coupled non-linear oscillators. In *International symposium on mathematical problems in theoretical physics*, pages 420–422. Springer, 1975.

[15] J. Machowski, J. Bialek, and J. R. Bumby. *Power System Dynamics: Stability and Control*. John Wiley & Sons, 2008.

[16] D. Manik, D. Witthaut, B. Schäfer, M. Matthiae, A. Sorge, M. Rohden, E. Katifori, and M. Timme. Supply networks: Instabilities without overload. *The European Physical Journal Special Topics*, 223(12):2527–2547, 2014.

[17] P. J. Menck, J. Heitzig, J. Kurths, and H. J. Schellnhuber. How dead ends undermine power grid stability. *Nature communications*, 5:3969, 2014.

[18] P. J. Menck, J. Heitzig, N. Marwan, and J. Kurths. How basin stability complements the linear-stability paradigm. *Nature Physics*, 9(2):89, 2013.

[19] A. E. Motter, S. A. Myers, M. Anghel, and T. Nishikawa. Spontaneous synchrony in power-grid networks. *arXiv preprint arXiv:1302.1914*, 2013.

[20] M. Newman. *Networks: an introduction*. Oxford university press, 2010.

[21] T. Nishikawa and A. E. Motter. Comparative analysis of existing models for power-grid synchronization. *New Journal of Physics*, 17(1):015012, 2015.

[22] J. Nitzbon, P. Schultz, J. Heitzig, J. Kurths, and F. Hellmann. Deciphering the imprint of topology on nonlinear dynamical network stability. *New Journal of Physics*, 19(3):033029, 2017.

[23] North American Electric Reliability Council. Review of selected 1996 electric system disturbances in north america. 2002.

[24] G. A. Pagani and M. Aiello. The power grid as a complex network: a survey. *Physica A: Statistical Mechanics and its Applications*, 392(11):2688–2700, 2013.

[25] A. Plietzsch, P. Schultz, J. Heitzig, and J. Kurths. Local vs. global redundancy – trade-offs between resilience against cascading failures and frequency stability. *The European Physical Journal Special Topics*, 225(3):551–568, 2016.

[26] H. Poincare. *Science and Method*. Thomas Nelson & Sons, 1914. (Translation by F. Maitland).

[27] F. A. Rodrigues, T. K. D. Peron, P. Ji, and J. Kurths. The kuramoto model in complex networks. *Physics Reports*, 610:1–98, 2016.

[28] G. Rogers. *Power system oscillations*. Springer Science & Business Media, 2012.

[29] P. Schultz, J. Heitzig, and J. Kurths. Detours around basin stability in power networks. *New Journal of Physics*, 16(12):125001, 2014.

[30] P. Schultz, J. Heitzig, and J. Kurths. A random growth model for power grids and other spatially embedded infrastructure networks. *The European Physical Journal Special Topics*, 223(12):2593–2610, 2014.

[31] K. Sun. Complex networks theory: A new method of research in power grid. In *Transmission and Distribution Conference and Exhibition: Asia and Pacific, 2005 IEEE/PES*, pages 1–6. IEEE, 2005.

[32] D. J. Watts and S. H. Strogatz. Collective dynamics of 'small-world' networks. *nature*, 393(6684):440, 1998.

[33] E. T. Whittaker and G. N. Watson. *A course of modern analysis*. Cambridge University Press, 1952.

Acknowledgement

I would like to offer my thanks to Jürgen Kurths and Frank Hellmann for supervising my thesis. Further, I want to thank the CoNDyNet team at PIK for their support, especially Jobst Heitzig, Paul Schultz, Sabine Auer and Maria Jarolin. I am grateful for the valuable comments and corrections of the final draft by Malte, Konrad and Michi. Finally, I wish to thank my parents, the Stutti11 crew and Luise.

Selbständigkeitserklärung

Ich erkläre ausdrücklich, dass es sich bei der von mir eingereichten schriftlichen Arbeit um eine von mir selbstständig und ohne fremde Hilfe verfasste Arbeit handelt.

Ich erkläre ausdrücklich, dass ich sämtliche in der oben genannten Arbeit verwendeten fremden Quellen als solche kenntlich gemacht habe. Insbesondere bestätige ich, dass ich ausnahmslos sowohl bei wörtlich übernommenen Aussagen als auch bei in eigenen Worten wiedergegebenen Aussagen anderer Autorinnen und Autoren (Paraphrasen) die Quelle angegeben habe.

Mir ist bewusst, dass Verstöße gegen die Grundsätze der Selbstständigkeit als Täuschung betrachtet und entsprechend der Prüfungsordnung und/oder der Allgemeinen Satzung für Studien- und Prüfungsangelegenheiten der HU (ASSP) geahndet werden.